AGU PUBLICATIONS

Global Biogeochemical Cycles

RESEARCH ARTICLE
10.1002/2015GB005187

Key Points:
- Isotope tracers and concentrations can predict N cycling rates
- Nitrate isotope profiles suggest a nitrate sink by denitrification
- Nitrite isotopes predict that up to 50% of nitrite is reoxidized

Correspondence to:
C. Buchwald,
cbuchwald@whoi.edu

Citation:
Buchwald, C., A. E. Santoro, R. H. R. Stanley, and K. L. Casciotti (2015), Nitrogen cycling in the secondary nitrite maximum of the eastern tropical North Pacific off Costa Rica, *Global Biogeochem. Cycles*, *29*, 2061–2081, doi:10.1002/2015GB005187.

Received 7 MAY 2015
Accepted 13 NOV 2015
Accepted article online 17 NOV 2015
Published online 15 DEC 2015

Nitrogen cycling in the secondary nitrite maximum of the eastern tropical North Pacific off Costa Rica

Carolyn Buchwald[1], Alyson E. Santoro[2], Rachel H. R. Stanley[1,3], and Karen L. Casciotti[4]

[1]Woods Hole Oceanographic Institution, Woods Hole, Massachusetts, USA, [2]Horn Point Laboratory, University of Maryland Center for Environmental Science, Cambridge, Maryland, USA, [3]Now at Wellesley College, Wellesley, Maryland, USA, [4]Stanford University, Stanford, California, USA

Abstract Nitrite is a central intermediate in the marine nitrogen cycle and represents a critical juncture where nitrogen can be reduced to the less bioavailable N_2 gas or oxidized to nitrate and retained in a more bioavailable form. We present an analysis of rates of microbial nitrogen transformations in the oxygen deficient zone (ODZ) within the eastern tropical North Pacific Ocean (ETNP). We determined rates using a novel one-dimensional model using the distribution of nitrite and nitrate concentrations, along with their natural abundance nitrogen (N) and oxygen (O) isotope profiles. We predict rate profiles for nitrate reduction, nitrite reduction, and nitrite oxidation throughout the ODZ, as well as the contributions of anammox to nitrite reduction and nitrite oxidation. Nitrate reduction occurs at a maximum rate of 25 nM d^{-1} at the top of the ODZ, at the same depth as the maximum rate of nitrite reduction, 15 nM d^{-1}. Nitrite oxidation occurs at maximum rates of 10 nM d^{-1} above the secondary nitrite maximum, but also in the secondary nitrite maximum, within the ODZ. Anammox contributes to nitrite oxidation within the ODZ but cannot account for all of it. Nitrite oxidation within the ODZ that is not through anammox is also supported by microbial gene abundance profiles. Our results suggest the presence of nitrite oxidation within the ETNP ODZ, with implications for the distribution and physiology of marine nitrite-oxidizing bacteria, and for total nitrogen loss in the largest marine ODZ.

1. Introduction

Fixed nitrogen (N), in the forms of ammonium (NH_4^+), dissolved organic nitrogen, nitrite (NO_2^-) and nitrate (NO_3^-), is the major limiting nutrient in much of the ocean, such that the supply of NO_3^-, the primary form of fixed N in subsurface waters, to the surface ocean controls the amount of primary productivity and subsequent carbon export from the surface ocean [*Eppley and Peterson*, 1979]. New fixed N enters the ocean through continental runoff, atmospheric deposition, and biological nitrogen fixation [*Codispoti et al.*, 2001]; fixed N is removed during denitrification and anammox in water column oxygen deficient zones (ODZs), where dissolved oxygen (O_2) concentrations fall below 10 nM [*Morrison et al.*, 1998; *Thamdrup et al.*, 2012], and anoxic marine sediments [*Christensen et al.*, 1987; *Devol*, 1991; *Thamdrup and Dalsgaard*, 2002]. The balance of the sources and sinks of fixed N dictates the oceanic N inventory and potential for carbon dioxide (CO_2) fixation and removal from the atmosphere. Historically, there has been disagreement among estimates of the marine fixed N budget, with some studies predicting that sinks vastly outweigh sources [*Brandes and Devol*, 2002; *Deutsch et al.*, 2004; *Codispoti et al.*, 2001]. However, most recent studies infer a balanced N budget [*Gruber and Sarmiento*, 1997; *Gruber and Galloway*, 2008; *DeVries et al.*, 2012, 2013; *Eugster and Gruber*, 2012]. There has also been active investigation into the rates and relative contributions of anammox and denitrification to fixed N removal [*Dalsgaard et al.*, 2003; *Kuypers et al.*, 2003, 2005; *Ward et al.*, 2009; *Lam et al.*, 2009]. Recent work shows that while instantaneous measurements of anammox and denitrification rates often yield complete dominance of one process over the other [*Dalsgaard et al.*, 2012], on a longer term average, the rates and contributions of anammox and denitrification are set by the flux and carbon to nitrogen ratio (C:N), respectively, of particulate organic matter supplied to ODZs [*Ward*, 2013; *Babbin et al.*, 2014; *Kalvelage et al.*, 2013; *Dalsgaard et al.*, 2012]. This is important because while anammox, an autotrophic metabolism, removes CO_2 from the water column, denitrification, typically a heterotrophic process, is a source of CO_2. While both processes remove fixed N, they have opposing effects on the global carbon cycle.

Both anammox and denitrification are inhibited by oxygen [*Dalsgaard et al.*, 2014] and are confined to regions of the Arabian Sea and eastern tropical Pacific, where large expanses of the water column contain

O_2 concentrations low enough ($<1\ \mu M$) to support microbial N reduction. These areas are linked to weak ventilation, limiting oxygen supply, and a high demand for O_2 resulting from increased productivity due to upwelling of nutrients, and the remineralization of sinking organic matter in the underlying water column [*Wyrtki*, 1962]. While these areas comprise only 0.1% of the global ocean volume, they account for up to 30% of all fixed N loss from the ocean [*Codispoti et al.*, 2001]. These areas are also unique in their accumulation of nitrite (NO_2^-) [*Codispoti*, 1986] and dynamic production and consumption of nitrous oxide (N_2O) [*Codispoti and Christensen*, 1985; *Naqvi et al.*, 1998; *Farias et al.*, 2009; *Babbin et al.*, 2015].

The Costa Rica upwelling dome (CRD) is a unique upwelling feature with a diameter of 150 to 300 km within the ETNP, at about 9°N and 89°W [*Wyrtki*, 1964]. The CRD was first observed in 1959 [*Broenkow*, 1965; *Wyrtki*, 1964] as a thin mixed layer and shallow thermocline within 10 m of the surface. The upwelling dome results from a cyclonic eddy formed by the Equatorial Countercurrent, the Costa Rica Current, and the North Equatorial Current [*Wyrtki*, 1964]. The surface water in the dome has a slightly lower temperature, reduced oxygen, and increased nutrients compared to surrounding waters, due to the upwelling of deep waters [*Thomas*, 1966]. In addition to the unique chemical and physical characteristics of the CRD, it has also been found to have a unique phytoplankton community composition. Recent studies of the CRD have shown that instead of being dominated by larger eukaryotic phytoplankton like most upwelling zones, the CRD has a high concentration of picophytoplankton, predominantly *Synechococcus* [*Saito et al.*, 2005]. The predominance of *Synechococcus* in the CRD leads to a reduced export ratio and relatively low export production despite relatively high primary productivity [*Stukel et al.*, 2013].

The water masses in the CRD include Equatorial Subsurface Water, above 900 m, and North Pacific Intermediate Water below. A well-developed ODZ, characteristic of the ETNP, exists within these two water masses. Accompanying the low oxygen at depth are also increased phosphate and nitrate concentrations due to organic matter remineralization, mostly within the Equatorial Subsurface Water [*Broenkow*, 1965]. Vertical profiles of nitrite concentrations in the CRD show that there are two distinct maxima, like those observed in other productive upwelling regions with intense oxygen minima [*Brandhorst*, 1959; *Broenkow*, 1965]. The shallow nitrite peak, called the primary nitrite maximum (PNM), exists below the chlorophyll maximum at the base of the euphotic zone [*Kiefer et al.*, 1976; *Zafiriou et al.*, 1992]. The secondary nitrite maximum (SNM) occurs within the oxygen deficient layer, and exists only where the water column is functionally anoxic (below 10 nM oxygen) [*Thamdrup et al.*, 2012].

Multiple processes may be involved in the production and consumption of nitrite in these features. In the PNM, ammonia oxidation and partial nitrate assimilation may be involved with nitrite production, while nitrite consumption may occur through nitrite oxidation or by nitrite assimilation by phytoplankton. Which mechanism dominates the production and maintenance of the PNM has been debated [*Lomas and Lipschultz*, 2006], with some evidence supporting production via ammonia oxidation [*Brandhorst*, 1959; *Olson*, 1981; *Hattori and Wada*, 1971; *Ward et al.*, 1982; *Santoro et al.*, 2013], other evidence supporting partial nitrate assimilation [*Collos*, 1998; *Kiefer et al.*, 1976; *Vaccaro and Ryther*, 1960]. A recent study based on nitrite isotope distributions suggests that the dominant PNM production mechanism may depend on location or depth in the water column [*Buchwald and Casciotti*, 2013] as has been suggested by earlier studies [*Dore and Karl*, 1996].

The nitrite formed in the anoxic SNM is most likely produced by dissimilatory nitrate reduction, which is inhibited by oxygen. Loss of nitrite can occur through further reduction to nitric oxide or ammonium or through reoxidation to nitrate. While reduction of nitrite to N_2 gas by denitrification or anammox is the most logical sink for nitrite in the ODZ, mounting evidence suggests that nitrite oxidation may play an unexpectedly large role in nitrogen cycling in and around ODZs [*Anderson et al.*, 1982; *Casciotti*, 2009; *Füssel et al.*, 2012; *Lam et al.*, 2011; *Casciotti et al.*, 2013]. Early models suggest that 39–60% of all nitrate reduced to nitrite in the oxygen deficient layer will be reoxidized on the edges [*Anderson et al.*, 1982], while direct measurements indicate nitrite oxidizing activity in the ODZ itself [*Füssel et al.*, 2012; *Lipschultz et al.*, 1990; *Beman et al.*, 2013; *Ganesh et al.*, 2015]. Understanding how different processes control nitrite production and consumption in the SNM has important implications for understanding the loss of fixed N through denitrification and anammox in the ODZ.

The N and oxygen (O) isotopes of nitrite and nitrate ($\delta^{15}N_{NO2\ or\ NO3}$ (‰ versus atmospheric N_2) = $(^{15}N/^{14}N_{NO2\ or\ NO3} \div {}^{15}N/^{14}N_{N2} - 1) \cdot 1000$; $\delta^{18}O_{NO2\ or\ NO3}$ (‰ versus Vienna Standard Mean Ocean Water) = $(^{18}O/^{16}O_{NO2\ or\ NO3} \div {}^{18}O/^{16}O_{VSMOW} - 1) \cdot 1000$) can be used to constrain the processes that produce and consume nitrite

and nitrate over long space and time scales within the ODZ, compared to instantaneous rate measurements. Each process imparts a distinct isotope effect leaving an imprint on the isotope ratio of the substrates and products of the reaction. For example, the dual isotopes of nitrate have been shown to be a powerful tracer of N cycling in the northern ETNP. As dissimilatory nitrate reduction has equal isotope effects for N and O isotope fractionation [*Granger et al.*, 2008], samples within an ODZ undergoing nitrate reduction should increase uniformly in $\delta^{15}N_{NO3}$ and $\delta^{18}O_{NO3}$. Samples that do not show a 1:1 correspondence of $\delta^{15}N_{NO3}$ and $\delta^{18}O_{NO3}$ increases are likely to have been affected by processes other than nitrate reduction. *Sigman et al.* [2005] defined $\Delta(15,18) = (\delta^{15}N_{NO3} - \delta^{15}N_{NO3,deep}) - {}^{15}\varepsilon/{}^{18}\varepsilon \times (\delta^{18}O_{NO3} - \delta^{18}O_{NO3,deep})$ as the horizontal deviation from a 1:1 line on a plot of $\delta^{18}O_{NO3}$ versus $\delta^{15}N_{NO3}$, starting from a uniform deep ocean $\delta^{15}N_{NO3}$ ($\delta^{15}N_{NO3,deep}$) of 5.5‰ and $\delta^{18}O_{NO3}$ ($\delta^{18}O_{NO3,deep}$) of 2.5‰. Nitrite oxidation can cause a deviation of nitrate isotopes from the 1:1 line, since it regenerates nitrate with distinct N and O isotopic signals [*Sigman et al.*, 2005; *Casciotti et al.*, 2013]. The O isotope signature of regenerated nitrate is set by equilibration of nitrite oxygen atoms with water and the addition of oxygen atoms from water during nitrite oxidation [*Buchwald and Casciotti*, 2010; *Buchwald et al.*, 2012]. The $\delta^{15}N$ of regenerated nitrate is affected by the $\delta^{15}N$ of nitrite and kinetic isotope fractionation during nitrite oxidation [*Casciotti*, 2009; *Buchwald and Casciotti*, 2010; *Casciotti et al.*, 2013]. Data of this kind have indicated that there are processes other than denitrification affecting nitrate in the ETNP, such as nitrite reoxidation or nitrogen fixation [*Sigman et al.*, 2005; *Casciotti and McIlvin*, 2007].

A new coupled tracer based on N isotopes in nitrate and nitrite, $\Delta\delta^{15}N = \delta^{15}N_{NO3} - \delta^{15}N_{NO2}$, has been used to determine where nitrite oxidation is important in the water column [*Casciotti*, 2009; *Casciotti et al.*, 2013]. Where nitrate reduction occurs in isolation, $\Delta\delta^{15}N$ should reflect the isotope effect for dissimilatory nitrate reduction to nitrite (15–25‰) [*Granger et al.*, 2008; *Kritee et al.*, 2012]. Where nitrite reduction occurs, the residual nitrite should have a higher $\delta^{15}N$, which lowers $\Delta\delta^{15}N$ to values near 10‰ [*Casciotti*, 2009]. Since nitrite oxidation has an inverse N isotope effect (−22 to −12‰) [*Casciotti*, 2009; *Buchwald and Casciotti*, 2010], its occurrence should lead to a depletion of ^{15}N in residual nitrite, leading to a larger $\Delta\delta^{15}N$ compared to where nitrate reduction and/or nitrite reduction dominate [*Casciotti*, 2009]. Applications of this tracer have suggested that nitrite oxidation may play a role in N cycling in and around the ODZs in the eastern tropical North Pacific [*Casciotti*, 2009], the eastern tropical South Pacific off the coast of Peru [*Casciotti et al.*, 2013; *Bourbonnais et al.*, 2015], and in the Arabian Sea [*Gaye et al.*, 2013].

The oxygen isotopes in nitrite contain additional information about the sources and cycling of nitrite in the ocean [*Buchwald and Casciotti*, 2013]. In addition to microbially mediated reactions, the oxygen isotopes in nitrite are affected by abiotic equilibration between nitrite oxygen atoms and water [*Buchwald and Casciotti*, 2013]. Because of this equilibration, $\delta^{18}O_{NO2}$ is altered from its biological source signature at a set rate until it reaches an equilibrated $\delta^{18}O$ value ($\delta^{18}O_{NO2,eq}$) set by that of the water $\delta^{18}O$ and equilibrium isotope effect ($^{18}\varepsilon_{eq}$) [*Casciotti et al.*, 2007]. The rate of this equilibration is dependent on ambient temperature and pH [*Buchwald and Casciotti*, 2013]. The $\delta^{18}O_{NO2}$ measurements have been used to analyze nitrite sources and cycling in the PNM, but similar studies have not yet been conducted in a SNM.

In the present study, we integrate $\delta^{15}N_{NO3}$, $\delta^{18}O_{NO3}$, $\delta^{15}N_{NO2}$, and $\delta^{18}O_{NO2}$ isotope measurements in a one-dimensional reaction diffusion model to determine the major nitrogen cycling processes affecting nitrate and nitrite distributions in the ETNP ODZ. By including advection and diffusion of nitrate and nitrite in and out of the oxygen deficient layer, we are able to test the impact of oxidation on the edges of the SNM on the nitrite and nitrate concentrations and isotopes in the feature. We also use a combination of molecular detection of nitrifying microorganisms and $^{15}NH_4^+$-based ammonia oxidation rate measurements to investigate the decoupling of nitrification processes associated with the ODZ. Together, this combination of experimental, observational, and modeling approaches has helped us gain a better understanding of the distribution of nitrification (ammonia oxidation and nitrite oxidation), dissimilatory nitrate reduction, denitrification, and anammox in the ETNP ODZ.

2. Methods

2.1. Ammonium, Nitrite, and Nitrate Concentration Measurements

All samples were collected aboard the Costa Rica Dome Flux and Zinc Experiment cruise in July 2010 aboard the R/V *Melville* (MV1008). During the 35 day cruise, we occupied five Lagrangian stations, referred to here as cycles, in which a parcel of water was tracked using a drifting array drogued at 100 m for 4 days. Figure 1 shows the

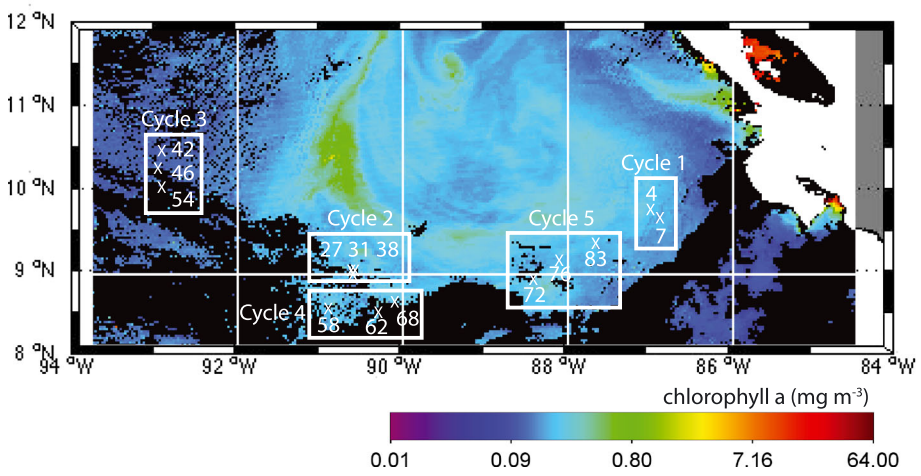

Figure 1. Map of cycle (labeled boxes) and hydrocast (numbered xs) locations during the cruise MV1008, superimposed on satellite image of chlorophyll a from 13 May 2010.

location of each numbered hydrocast, within boxes indicating the cycle each cast was associated with. The hydrocast locations within a cycle could be far apart, depending on the surface currents at each cycle. In each cycle, two or three 24-depth profiles of nutrient and isotope samples were collected. Cycles 2 and 4 were located within the upwelling dome, cycle 5 was at the edge of the dome, cycle 3 was outside the dome in open ocean waters, and cycle 1 was outside the dome in coastal waters.

Dissolved oxygen was measured on each hydrocast using a Seabird SBE 43 sensor attached to a conductivity-temperature-depth on a Niskin rosette. Its detection limit is 1–5 μM, with a precision of 1.5 μM. The ODZ used here to designate waters with oxygen concentrations below the detection limit of the sensor was 200 m thick in cycles 2, 4, and 5, spanning from 400 to 600 m depth (Figure 2a). In cycle 1, which was closest to shore, the ODZ occurred slightly shallower in the water column spanning from 350 to 550 m. In cycle 3, the farthest offshore, the oxygen deficient zone was 300 m thick, spanning from 400 to 700 m (Figure 2a).

Ammonium and nitrite concentrations were measured aboard the ship immediately after collection. Nitrite measurements were made using the Greiss-Ilosvay colorimetric method [*Strickland and Parsons*, 1972]. Samples (10 mL) were collected in 15 mL centrifuge tubes and 100 μL of sulfanilamide (SAN, 0.5 g L^{-1}) and N-(1-naphthyl)ethylenediamine (NED, 0.05 g L^{-1}) were added. Then 1 mL of each sample was analyzed on

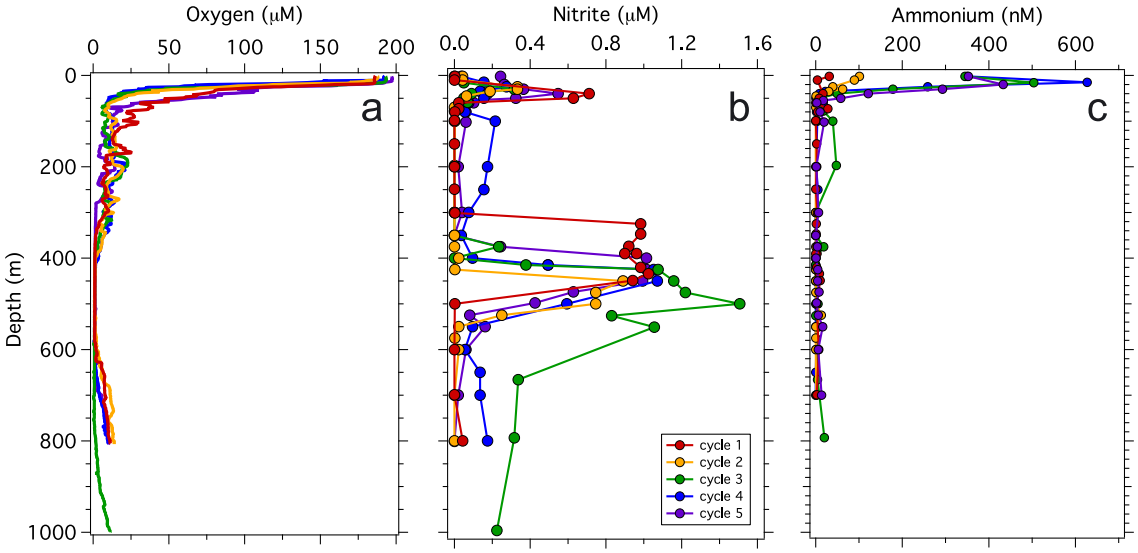

Figure 2. Depth profiles of (a) oxygen, (b) nitrite, and (c) ammonium concentrations from the five cycles with locations shown in Figure 1.

a spectrophotometer. Bracketing standards (0 to 5 μM NO_2^-) were run in parallel and then used to calculate the concentration in each sample. The nitrite detection limit using this method is 0.2 μM.

Ammonium was measured using the orthophthaldehyde (OPA) method [*Holmes et al.*, 1999] with a detection limit of 10 nM. For these measurements, 40 mL samples were collected in 60 mL high-density polyethylene (HDPE) sample bottles. Bottles were acid washed prior to first use and then preconditioned with a small amount of OPA reagent prior to use to remove any ammonium contamination. Sample bottles sat with the last seawater sample and reagent between casts and were emptied just prior to rinsing and subsequent sample collection on the following cast. Along with the samples, 10 bottles were used to run five standards in duplicate ranging from 0 to 0.5 μM ammonium. Standards were made by collecting water from below 1000 m into the HDPE bottles and then adding small volumes of a 50 μM NH_4Cl stock solution that was stored at 4°C. New standards were made for each cast. Ten milliliters of OPA reagent was added to each sample and standard bottle and then allowed to react in the dark for 3–10 h. With each batch of samples, one deepwater sample had reagent added just before measurement on the fluorometer. This fluorescence value was used as a matrix blank and subtracted from all of the other samples. Fluorescence was measured for each sample and standard using a handheld fluorometer (Turner Aquafluor 8000).

Nitrate concentration measurements were done using a WestCo 200 discrete analyzer in the Stanford University Environmental Measurement 1: Gas-Solution Analytical Center. The discrete analyzer is an automated spectrophotometer that first reduces nitrate to nitrite using a cadmium column and then reacts the resulting nitrite with SAN and NED using the Greiss-Islovay method, as above. Because nitrate conversion to nitrite can be incomplete using this method (here averaged ~70%), nitrate and nitrite standard curves were analyzed with each batch of samples in order to calibrate samples that contained both nitrite and nitrate. This was done by subtracting the absorbance due to nitrite from the total absorbance, using the measured nitrite concentration and the nitrite standard curve produced by the discrete analyzer. The resulting nitrite-corrected absorbance value was then calibrated using the nitrate standard curve to find the nitrate concentration.

2.2. Ammonia Oxidation Rate Measurements

Ammonia oxidation rates were measured by conducting $^{15}NH_4^+$ incubations at three depths at each of cycles 2, 3, and 4. The depths chosen targeted the surface (with O_2 concentrations near 210 μM), PNM (with O_2 between 78 and 182 μM) and at the oxycline (with O_2 concentrations decreasing to ~6 μM O_2 just above the SNM). For the two shallowest (oxygenated) depths, incubations were conducted in clear 500 mL polycarbonate bottles (Nalgene). The oxycline incubations were conducted in 500 mL Tedlar bags prepurged with N_2 gas and equipped with three-way stopcocks for gas tight additions and subsampling. While we cannot rule out oxygen contamination of the Tedlar bags, ammonia oxidation rates have been shown to be insensitive to variations in O_2 concentration at these levels [*Füssel et al.*, 2012]. Two incubation treatments were conducted in duplicate at each depth for a total of four bottles or bags: (1) whole seawater and (2) 0.2 μm filtered control. All four bottles received 0.5 mL of 99.5 atom% ^{15}N-labeled NH_4Cl (Cambridge Isotope Laboratory), for a tracer addition of 5 μM in the oxic depths and 0.2 μM in the deepest anoxic depth, corresponding to final atom% ^{15}N enrichments of 87.8 to 99.5%.

Incubations were conducted as close to in situ light and temperature conditions as possible. The surface samples were incubated in a blue translucent on-deck incubator with running surface seawater for temperature control. The PNM incubations were conducted in the same incubator but wrapped in neutral density screening to simulate 1% surface irradiance. The deepest samples were incubated in the dark in an incubator adjusted to 10°C. Sixty milliliters of water was subsampled from each bottle at four time points: 0, 12, 24, and 36 h, then 0.2 μm syringe filtered (Sterivex) and frozen for later $\delta^{15}N_{NO2+NO3}$ analysis. The $\delta^{15}N_{NO2+NO3}$ was measured using the denitrifier method, described below, except that nitrite was not removed. Ammonia oxidation rates were calculated from the time course changes in $\delta^{15}N_{NO2+NO3}$, according to *Santoro et al.* [2013]. All fitting was done using nonlinear least squares in MATLAB.

2.3. DNA Extraction and Quantitative PCR (qPCR)

Water samples were collected from four to five depths in each cycle to measure the abundance of nitrifying organisms using quantitative polymerase chain reaction (qPCR) assays for the ammonia monooxygenase subunit A gene (*amoA*) from ammonia-oxidizing bacteria (AOB) and archaea (AOA) and the 16S ribosomal RNA (rRNA) gene of the nitrite-oxidizing bacterial genus *Nitrospina*. Water was collected at the surface, PNM,

SNM, middle of the ODZ, and at the bottom edge of the ODZ where oxygen concentrations begin to increase below the zone of anoxia. Samples for DNA analysis were collected on 25 mm, 0.2 μm pore size Supor filters (Pall) using pressure filtration with a peristaltic pump; 1 L of seawater was filtered from the surface waters and 4 L for the deeper samples. Filters were immediately transferred to a 1.5 mL sterile gasketed bead beating tube, which was prefilled with 30 μL of 0.1 mm glass beads (BioSpec) and frozen in a −80°C freezer. A total of 29 samples were collected for molecular analysis. Due to the time sensitivity of sample processing for DNA samples and rate measurements, these samples were collected on separate casts from the incubations within a given cycle.

DNA extraction followed the method of *Santoro et al.* [2010]. Briefly, 750 μL of alkaline sucrose ethylenediaminetetra-acetic acid lysis buffer and 100 μL 10% sodium dodecyl sulfate were added to the tubes containing the frozen filter and processed in a bead beater (BioSpec) for 1.5 min. Following bead beating, tubes were incubated in boiling water for 1 min and then 50 μL of 20 mg mL^{-1} proteinase K (New England BioLabs) was added and incubated at 55°C for 2–4 h. Each tube was then centrifuged to remove debris and the supernatant was transferred to a clean tube. The filter debris was washed once with 100 μL lysis buffer to remove any remaining DNA and was centrifuged, and supernatant was combined with the initial lysate. Lysates were purified using the DNeasy spin columns (Qiagen) following manufacturer's protocol. DNA was eluted in 150 or 200 μL of nuclease-free water and quantified using a Qubit fluorometer (Life Technologies).

The qPCR was carried out in 20 μL reactions, made of 10 μL Mastermix (Bio-Rad ssoAdvanced SYBR), 200 nM of each primer, 1 μL of template, and 8.4 μL of RNase free water. Samples and no template controls were analyzed in triplicate along with duplicate sets of standards with 10 to 10^5 templates on a Bio-Rad CFX96 real-time PCR machine. The betaproteobacterial *amoA* qPCR assay used the 1F/2R primer set [*Rotthauwe et al.*, 1997]. The archaeal *amoA* assay used the Arch-amoAF/Arch-amoAR set with an additional 2 mM $MgCl_2$ [*Francis et al.*, 2005]. Lastly, *Nitrospina*-like 16S rRNA genes were quantified using the primers NitSSU_130F and NitSSU_282F [*Mincer et al.*, 2007]. Efficiencies of the three assays were 92%, 83%, and 95%, respectively.

2.4. Nitrite and Nitrate Isotope Measurements

The $\delta^{15}N_{NO2}$ and $\delta^{18}O_{NO2}$ were measured using the azide method [*McIlvin and Altabet*, 2005]. All of the samples were prepared in duplicate 20 mL glass vials, and nitrite was converted to N_2O on board the ship, as soon as possible after sampling (generally within 1 h), to limit the abiotic exchange of oxygen atoms between nitrite and water [*Casciotti et al.*, 2007]. Using the nitrite concentration (measured on board as above), the volume of sample needed to make 2.5, 5, or 10 nmol of N_2O was calculated and added to each vial. Nitrite isotope standards N-23, N-7373, N-10219 [*Casciotti et al.*, 2007] were prepared and analyzed in parallel, with triplicate aliquots of each standard bracketing the nanomole amounts of the batch of samples. The azide reagent was added to each sample and standard at a ratio of 100 μL to 3 mL of sample. After 30 min, 6 M NaOH was added to each vial in a volume equal to the azide reagent to stop the reaction. The resulting N_2O was stored at room temperature in the septum-sealed vials for 4 weeks prior to analysis on a Finnigan Delta^{PLUS} XP isotope ratio mass spectrometer.

Approximately 60 mL of seawater from each depth was 0.2 μm filtered and frozen for nitrate isotope analysis in the laboratory. Nitrate isotope samples were analyzed in duplicate using the denitrifier method [*Casciotti et al.*, 2002; *Sigman et al.*, 2001] with minor modifications [*McIlvin and Casciotti*, 2011]. In samples containing detectable levels of nitrite (>0.2 μM), nitrite was removed using sulfamic acid [*Granger and Sigman*, 2009] prior to analysis by the denitrifier method. In this way, nitrate isotopic measurements are uncontaminated by nitrite. Three nitrate isotope standards, U.S. Geological Survey (USGS)32, USGS34, and USGS35 [*Bohlke et al.,* 2003], were each run 6 times per 60 samples at two different nmol amounts (5 and 20 nmol of N) to correct for differential blank effects in samples of varying sizes (nmol N). Typical standard deviation nitrate and nitrite isotope measurements are 0.2‰ for $\delta^{15}N$ and 0.5‰ for $\delta^{18}O$.

3. Results

3.1. Nutrient Profiles in the CRD

Nitrite showed both primary (PNM) and secondary (SNM) maxima at each cycle (Figure 2b). The PNM occurred between 20 and 40 m at every cycle. The highest [NO_2^-] measured in the PNM was 1.3 μM in cycle 1. Lower

concentrations of 0.6 to 0.8 μM were measured in cycles 2, 4, and 5. Sampling using the Niskin bottles to capture this narrow feature was difficult, though, and the apparently lower nitrite concentrations at cycles 2, 4, and 5 could have resulted from missing the peak nitrite concentration within the PNM. The stations sampled had a range of nitrite concentrations in the SNM of 1–1.6 μM, with the largest SNM at cycle 3 (the farthest offshore). Cycle 3 also had the largest vertical extent of nitrite in the water column, where it extended all the way to 1000 m, and the largest vertical extent of the ODZ (Figure 2b). The lowest concentration and depth range of the SNM were measured at cycles 2 and 4. These stations also had the smallest ODZ.

Ammonium concentration profiles showed distinct maxima of up to 0.6 μM directly above the PNM (Figure 2c). There was also up to 0.35 μM ammonium at the surface. The cycle closest to shore (cycle 1) had the lowest ammonium concentration, with a 0.10 μM peak just above the PNM. In addition to the near-surface ammonium maximum, there appears to be a small secondary ammonium maximum of 0.02–0.04 μM (just above the detection limit) at the bottom edge of the ODZ in cycles 2, 3, and 5 (Figure 2c). This peak is most visible in cycle 5, with at least three samples defining the ammonium peak at the bottom edge of the ODZ from 480 to 600 m. Ammonium was below detection limits within the ODZ.

The nitrate profiles (not shown) followed a typical nutrient-like distribution in the upper water column. Nitrate was depleted but detectable (~1 to 2 μM) at the surface and increased with depth to ~45 μM at 800 m. There were midwater column dissolved inorganic nitrogen (DIN) deficits (DIN deficit (μM) = $([NO_2^-] + [NO_3^-]) - 16 \times [PO_4^{3-}] + 2.9$) calculated for cycles 3–5 (not shown). DIN deficits of up to 26 μM occurred between 400 and 420 m and were associated with the upper 100 m of the ODZ.

3.2. Ammonia Oxidation Rates in the CRD

Ammonia oxidation rates were measured at three depths (surface, PNM, and just above the SNM) at each of three locations (cycles 2, 3, and 4) (Figures 3a–3c, LHS). Overall, the rates were low, showing a maximum rate of ~3 nM d^{-1}. There was no measurable ammonia oxidation (<0.005 nM d^{-1}) in the surface (2 m) at any of the cycles. In cycle 2, the highest rate of ammonia oxidation occurred at the PNM, with a slightly lower rate observed in the oxycline above the SNM. In cycles 3 and 4, the highest rate of ammonia oxidation occurred within the oxycline, with a much lower rate observed at the PNM. Filtering almost always completely eliminated ammonia oxidation, except for the two locations where the rates were highest (cycle 2 (PNM) and cycle 3 (oxycline)).

3.3. Nitrifying Organism Abundance

There was a low abundance (~10 copies mL^{-1}) of AOB throughout the water column in all cycles (Figures 3a–3e, RHS). In all surface samples, AOA were near the detection limit (<0.01 copies mL^{-1}). At cycle 1, the highest abundance of AOA (~5000 copies mL^{-1}) was measured in the PNM, with a lower abundance in the deeper samples. AOA abundance in the PNM decreased in the offshore stations. At cycles 3–5, the maxima in archaeal *amoA* abundance occurred in the oxycline near the bottom of the ODZ. *Nitrospina* 16S rRNA gene abundance was also highest in the PNM (4360 copies mL^{-1}) at cycle 1. Interestingly, cycles 2–5 showed peak *Nitrospina* abundances (910–1680 copies mL^{-1}, respectively) at O_2 concentrations below 10 μM in the oxycline and ODZ. *Nitrospina* abundances were also high within the ODZ at cycle 1. In cycles 1 and 2, the AOA abundance was greater than the *Nitrospina* in the PNM but smaller throughout the ODZ. In cycles 3, 4, and 5, *Nitrospina* abundance was greater than AOA everywhere in the profile.

3.4. Multi-isotope Profiles ($\delta^{15}N_{NO2}$, $\delta^{18}O_{NO2}$, $\delta^{15}N_{NO3}$, $\delta^{18}O_{NO3}$, Δ(15,18), and $\Delta\delta^{15}N$)

The isotopes of nitrate ($\delta^{15}N_{NO3}$ and $\delta^{18}O_{NO3}$) and nitrite ($\delta^{15}N_{NO2}$ and $\delta^{18}O_{NO2}$) were measured in depth profiles in cycles 2–5. Using these isotope values, two different tracers were calculated, $\Delta(15,18)$ (‰) = $(\delta^{15}N_{NO3} - 5.5) - (\delta^{18}O_{NO3} - 2.5)$ and $\Delta\delta^{15}N$ (‰) = $\delta^{15}N_{NO3} - \delta^{15}N_{NO2}$. Figure 4 includes the profiles of all four isotope ratios ($\delta^{15}N_{NO3}$, $\delta^{18}O_{NO3}$, $\delta^{15}N_{NO2}$, and $\delta^{18}O_{NO2}$) and their derived tracers ($\Delta(15,18)$, $\Delta\delta^{15}N$) for casts 72, 76, and 83 from cycle 5. Among our data, these profiles had highest resolution of sampling within the ODZ. Data from other cycles showed similar patterns. The $\delta^{15}N_{NO3}$ and $\delta^{18}O_{NO3}$ followed the patterns roughly expected for this location, with values of both increasing to 15–20‰ in surface waters and within the ODZ, and reaching deepwater values of 5.5‰ and 2.5‰, respectively, similar to earlier studies [*Sigman et al.*, 2009; *Rafter et al.*, 2013]. High $\delta^{15}N_{NO3}$ and $\delta^{18}O_{NO3}$ values in the surface most likely result from assimilation of nitrate by phytoplankton, whereas in the ODZ, it is caused by dissimilatory nitrate reduction. Both of these processes have equal isotope effects for ^{15}N and ^{18}O and should cause equal variations in $\delta^{15}N_{NO3}$

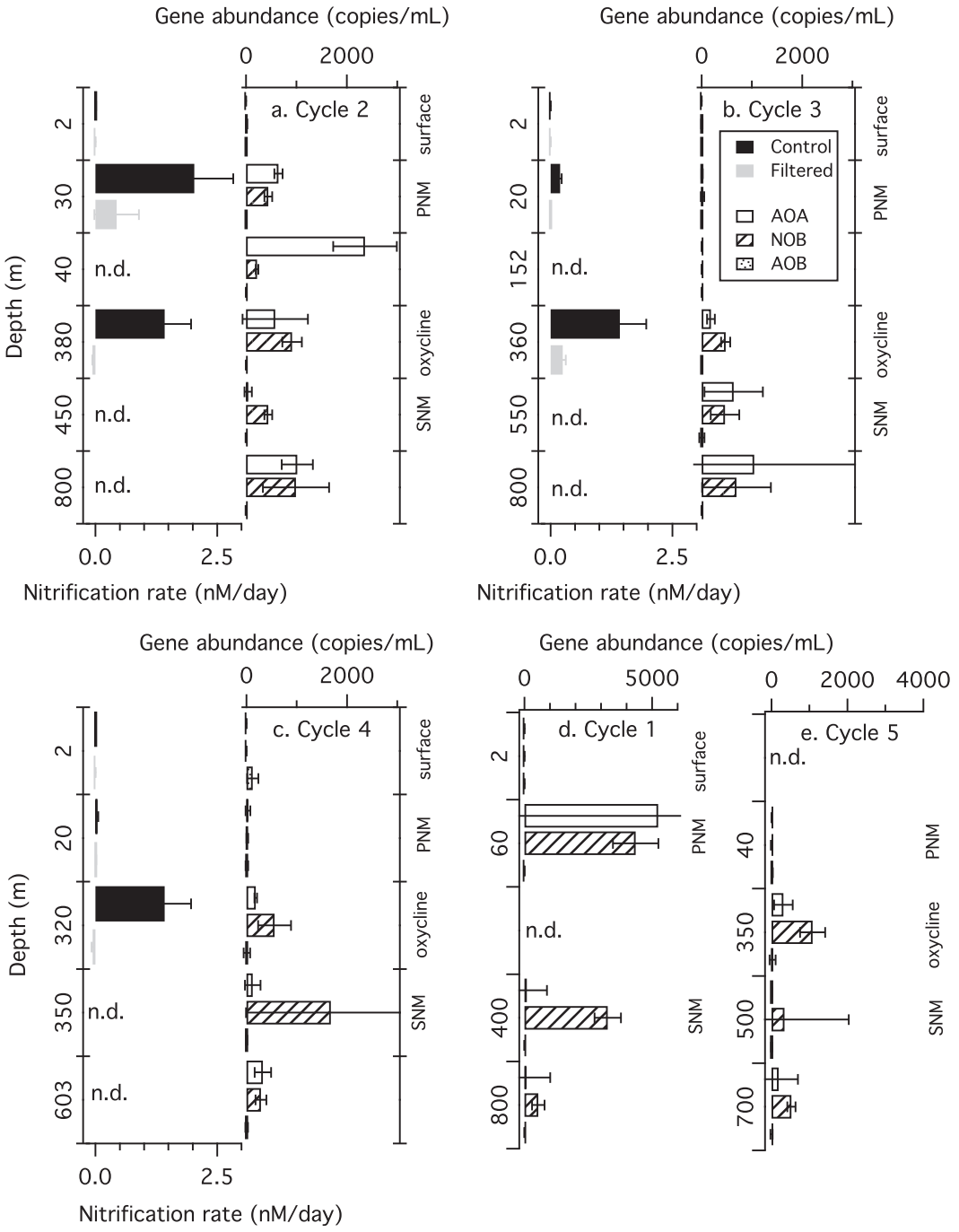

Figure 3. Ammonia oxidation rates measured in bottle incubations at three depths are shown for (a–c) cycles 2–4 (LHS). Gene abundance of AOA, AOB, and *Nitrospina*-like NOB measured from qPCR and are shown for (a–e) cycles 1-5 (RHS). Rates not determined are indicated by n.d. Note that the depths shown on the *y* axis are shown as categories, arranged in order of depth, rather than a continuous depth scale.

and $\delta^{18}O_{NO3}$, yielding Δ(15,18) values near 0‰ (no deviation from the 1:1 correspondence of $\delta^{15}N_{NO3}$ and $\delta^{18}O_{NO3}$) [*Granger et al.*, 2008, 2010; *Sigman et al.*, 2005]. Despite the expected increases in $\delta^{15}N_{NO3}$ and $\delta^{18}O_{NO3}$ in the surface and ODZ, there were three depths in the water column that had large negative Δ(15,18) values: the surface, at the top of the upper oxycline, and in the lower oxycline. The areas with these negative deviations indicate the influence of nitrate-regenerating processes [*Sigman et al.*, 2005; *Wankel et al.*, 2007; *Casciotti and McIlvin*, 2007; *Casciotti et al.*, 2013] that will be explored below in more detail.

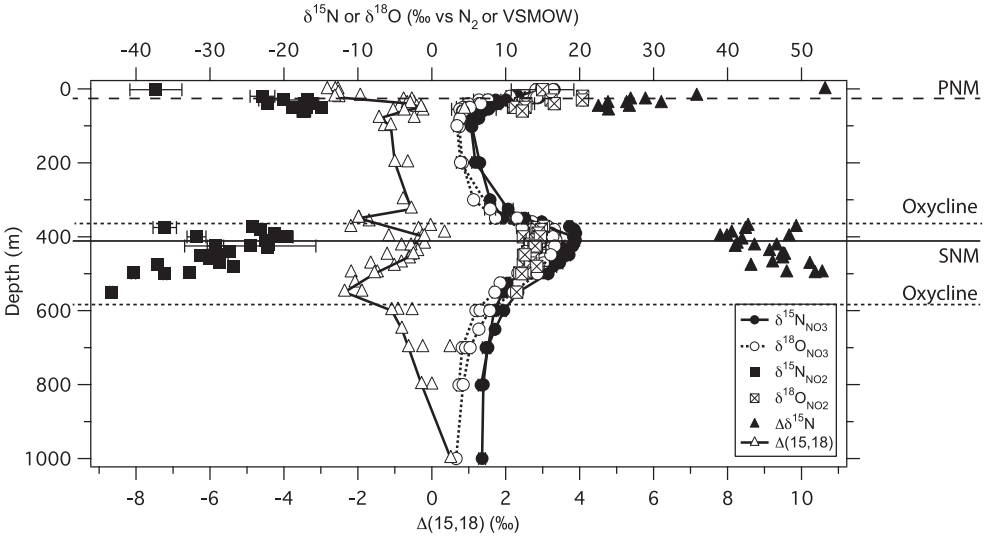

Figure 4. Depth profiles of nitrite isotope ($\delta^{15}N_{NO2}$ and $\delta^{18}O_{NO2}$), nitrate isotope ($\delta^{15}N_{NO3}$ and $\delta^{18}O_{NO3}$), Δ(15,18), and $\Delta\delta^{15}N$ ($\delta^{15}N_{NO3} - \delta^{15}N_{NO2}$) from casts 72, 76, and 83 in cycle 5. The dashed line indicates the location of the PNM, the dotted lines indicate the top (where oxygen reaches its minimum concentration) and bottom (where oxygen begins to increase above its minimum level) of the ODZ, and the solid line indicates the location of the SNM peak. The error bars representing ±1 standard deviation of measurement or propagated error are included for each data set and are generally smaller than the symbols.

The $\delta^{15}N_{NO2}$ values in the PNM were lowest (–38‰) near the surface and increased with depth to -15‰ (Figure 4). The $\delta^{15}N_{NO2}$ values within the SNM followed the shape of the nitrite concentration profile—$\delta^{15}N_{NO2}$ was lowest on the bottom edge of the feature (–45‰) and increased to –20‰ at the peak of the SNM and then decreased again toward the top of the ODZ where nitrite goes to zero. The $\Delta\delta^{15}N$ ($\delta^{15}N_{NO3} - \delta^{15}N_{NO2}$) had a distribution opposite that of $\delta^{15}N_{NO2}$ (Figure 4) and nitrite concentration (Figure 2b). The highest values of $\Delta\delta^{15}N$ (over 50‰) coincided with the lowest nitrite concentrations, lowest $\delta^{15}N_{NO2}$, and most negative Δ(15,18) in both the PNM and SNM (Figure 4). The lowest values of $\Delta\delta^{15}N$ (near 20‰) occurred below the PNM where nitrite concentrations have almost returned to background levels.

The $\delta^{18}O_{NO2}$ values had a more homogenous profile than any other tracer. In both the PNM and SNM, the $\delta^{18}O_{NO2}$ showed a distribution similar to that of $\delta^{15}N_{NO2}$ but with a much smaller range of values. The average $\delta^{18}O_{NO2}$ values were 14.7‰ in the primary nitrite maximum and 13.4‰ in the SNM. These values are close to those expected after equilibration of nitrite and water (with a $\delta^{18}O_{H2O}$ of 0‰) at in situ temperatures (average $\delta^{18}O_{NO2,eq} = 14.0$‰) [*Casciotti et al.*, 2007; *Buchwald and Casciotti*, 2013].

4. Discussion: Nitrogen Cycling in the SNM

At all of the stations in the ETNP, there was an SNM occurring within the ODZ, with nitrite concentrations peaking between 1.0 and 1.6 μM. The SNM has been classically assumed to arise from an imbalance of the reductive pathways nitrate reduction and nitrite reduction [*Codispoti and Christensen*, 1985], as this feature occurs only within functionally anoxic water columns [*Thamdrup et al.*, 2012]. *Anderson et al.* [1982] first suggested that nitrite produced in the ODZ could be transported to the fringes of the ODZ, where it would be reoxidized to nitrate and transported back into the ODZ. The reaction diffusion model used by Anderson suggests that 39 to 60% of the nitrite produced in the ODZ may be reoxidized to nitrate rather than being reduced to N_2 gas. They also found that nitrite oxidation helped explain the shape of the SNM (confining it to anoxic waters) and the nitrate deficit [*Anderson et al.*, 1982]. Nitrite oxidation helps define the shape of the SNM because if nitrite reduction was the only sink for nitrite, diffusion would lead to nitrite extending beyond the boundaries of the oxygen deficient waters. Instead, a very narrow peak with a steep decline on the top edge of the SNM is often observed, which can be explained by having a secondary sink of nitrite at the edges of the reduction zones. A similar degree of nitrite reoxidation was inferred from nitrate and nitrite isotopes in the Peruvian ODZ in the eastern tropical South Pacific Ocean where nitrite and nitrate

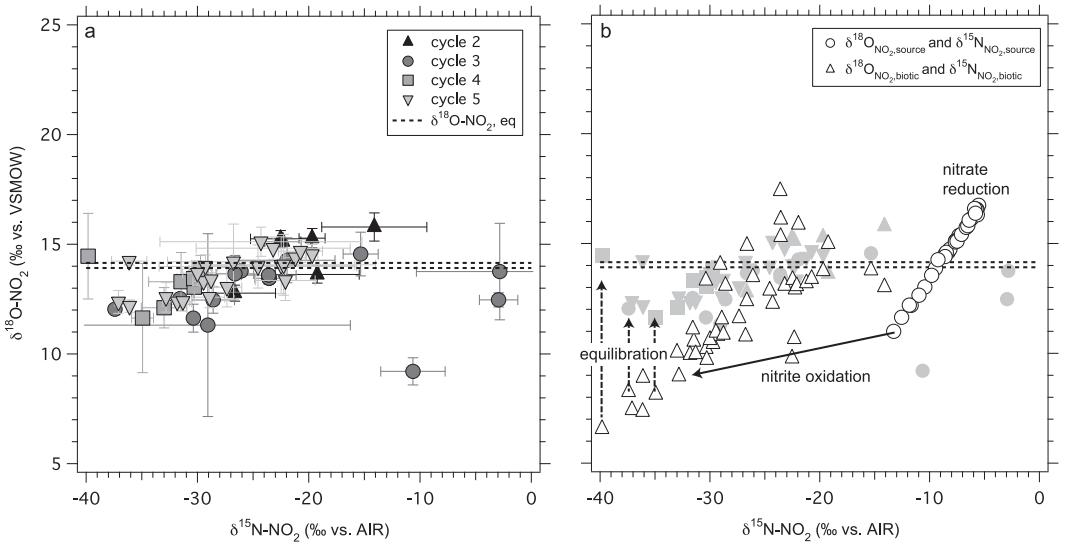

Figure 5. (a) The $\delta^{18}O_{NO2}$ and $\delta^{15}N_{NO2}$ data from the SNM from all cycles with error bars indicating ±1 standard deviation of measurements and (b) interpretation of nitrite isotope data (grayed out, with error bars removed) relative to sources and sinks of nitrite in the SNM. The expected $\delta^{15}N_{NO2}$ and $\delta^{18}O_{NO2}$ values produced from nitrate reduction ($\delta^{15}N_{NO2,source}$ and $\delta^{18}O_{NO2,source}$, respectively) are shown with open circles. The isotope effects of nitrite consumption by nitrite oxidation (solid arrow labeled "nitrite oxidation") and abiotic equilibration of oxygen isotopes between nitrite and water (dashed arrows labeled "equilibration") are shown. The open triangles represent the expected $\delta^{15}N_{NO2}$ and $\delta^{18}O_{NO2}$ after biological nitrite production and nitrite consumption (here assumed to be nitrite oxidation) prior to abiotic equilibration between nitrite and water. The dashed lines indicate the range of expected $\delta^{18}O_{NO2}$ values at equilibrium with the ambient $\delta^{18}O_{H2O}$.

isotope distributions were interpreted to reflect the activity of nitrite oxidation [*Casciotti et al.*, 2013]. However, in that study it was suggested that nitrite oxidation may also occur within the ODZ, in concert with nitrate and nitrite reduction. Here we address the issue of nitrite oxidation within the ETNP ODZ based on data gathered from molecular detection of nitrite-oxidizing organisms and multiple natural abundance isotopic tracers interpreted using a newly developed nitrogen isotope-enabled 1-D biogeochemical model.

4.1. SNM Nitrogen Cycling: Nitrite Oxygen Isotope Disequilibrium

The $\delta^{15}N_{NO2}$ and $\delta^{18}O_{NO2}$ values from the SNM can be used to infer the sources and rates of nitrite cycling in much the same way as for the PNM [*Buchwald and Casciotti*, 2013] but using a different set of sources and sinks. In the SNM, anoxic processes including dissimilatory nitrate reduction, nitrite reduction, and anammox, as well as nitrite reoxidation are considered. Figure 5a shows the nitrite isotope values for every sample collected from the SNM in this study. The $\delta^{15}N_{NO2}$ values ranged from −5‰ to −40‰, while $\delta^{18}O_{NO2}$ had a much narrower range, from 10 to 20‰. The most probable source of nitrite in the SNM is dissimilatory nitrate reduction. Consistent with this assumption, the DIN deficit and increases in $\delta^{15}N_{NO3}$ and $\delta^{18}O_{NO3}$ in the SNM also indicate that nitrate reduction has affected nitrate distributions in the ODZ. The $\delta^{15}N_{NO2}$ and the $\delta^{18}O_{NO2}$ values that would result from this process, based on $\delta^{15}N_{NO3}$ and $\delta^{18}O_{NO3}$ values for each sample, are shown in Figure 5b ($\delta^{15}N_{NO2,source}$ and $\delta^{18}O_{NO2,source}$; open circles). These nitrite isotope values were calculated by subtracting the isotope effects for nitrate reduction ($^{15}\varepsilon_{NAR} = {}^{18}\varepsilon_{NAR} = 25‰$) [*Granger et al.*, 2008] from the $\delta^{15}N_{NO3}$ and $\delta^{18}O_{NO3}$ values: $\delta^{15}N_{NO2,source} = \delta^{15}N_{NO3} - {}^{15}\varepsilon_{NAR}$ and $\delta^{18}O_{NO2,source} = \delta^{18}O_{NO3} - {}^{18}\varepsilon_{NAR} + {}^{18}\varepsilon_{b}$. For $\delta^{18}O$, a branching isotope effect ($^{18}\varepsilon_{b}$) of 25‰ was also applied [*Casciotti et al.*, 2007], yielding zero net fractionation between the available nitrate and the nitrite produced from it. This calculation yields predicted $\delta^{15}N_{NO2}$ values falling between −5‰ and −15‰ and $\delta^{18}O_{NO2}$ values falling between 10‰ and 17‰.

The majority of samples in the SNM had $\delta^{15}N_{NO2}$ values between −15‰ and −40‰, indicating that additional processes are needed to explain the nitrite isotope distribution in the SNM. If nitrite reduction was the only sink, $\delta^{15}N_{NO2}$ would either stay the same or become more enriched in ^{15}N because this process has a normal isotope effect (0–15‰) [*Bryan et al.*, 1983; *Casciotti et al.*, 2013; *Brunner et al.*, 2013; *Bourbonnais et al.*, 2015]. There were only three samples (600–1000 m at cycle 3) that had $\delta^{15}N_{NO2}$ values higher than the source, indicating that there may have been removal through nitrite reduction (Figure 5b). Nitrite oxidation leads to progressive

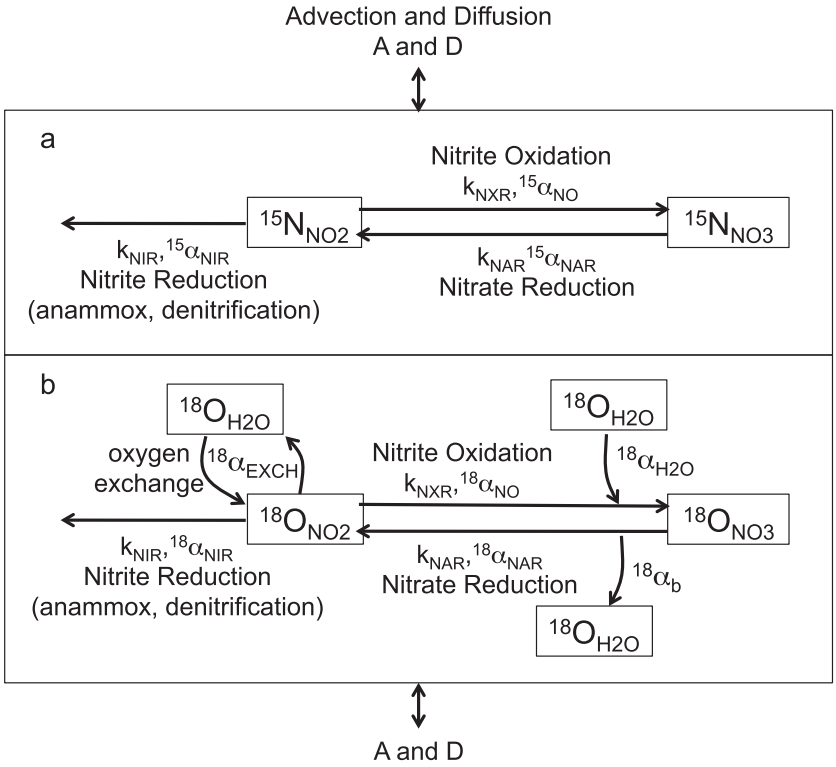

Figure 6. Depiction of processes included in the 1-D model to analyze the distributions of nitrate and nitrite concentrations and isotopes in the SNM. Main processes considered were nitrate reduction (NAR), nitrite reduction (NIR), nitrite oxidation (NXR), abiotic exchange of nitrite O atoms (EXCH), vertical advection (A), and diffusion (D). Biological processes were treated as first order rate equation with rate constants (k_{NAR}, k_{NIR}, and k_{NXR}) and kinetic isotope fractionation factors ($^{15}\alpha_{NAR}$, $^{18}\alpha_{NAR}$, $^{15}\alpha_{NIR}$, $^{18}\alpha_{NIR}$, $^{15}\alpha_{NXR}$, $^{18}\alpha_{NXR}$, $^{18}\alpha_{H2O}$, and $^{18}\alpha_b$, defined in the text). The abiotic process of oxygen isotope exchange was modeled with a first order rate constant (k_{EXCH}) and with equilibrium fractionation factor ($^{18}\alpha_{EXCH}$).

depletion of ^{15}N, and to a lesser extent ^{18}O, in residual nitrite because of inverse isotopic fractionation [*Casciotti*, 2009; *Buchwald and Casciotti*, 2010]. Based on measured N and O isotope effects for nitrite oxidation, −9 to −20‰ and −1 to −8‰, respectively [*Buchwald and Casciotti*, 2010], $\delta^{15}N_{NO2}$ and $\delta^{18}O_{NO2}$ should decrease along lines with a slope of 0.1, shown as a solid arrow in Figure 5b. Assuming that nitrite oxidation is the only sink for nitrite in the samples with observed $\delta^{15}N_{NO2}$ values below their $\delta^{15}N_{NO2,source}$, the expected $\delta^{18}O_{NO2}$ value at the observed $\delta^{15}N_{NO2}$, prior to oxygen atom equilibration, is given by $\delta^{18}O_{NO2,biotic}$ (Figure 5b, open triangles). The $\delta^{18}O_{NO2,biotic}$ reflects the $\delta^{18}O_{NO2}$ value that would be generated by the action of biological processes upon which abiotic equilibration acts. Oxygen atom equilibration between nitrite and water brings $\delta^{18}O_{NO2}$ to equilibrium (Figure 5b, dashed lines) without changing $\delta^{15}N_{NO2}$ [*Buchwald and Casciotti*, 2013]. Many of these $\delta^{18}O_{NO2,biotic}$ values fall near equilibrium making it difficult to resolve the age of nitrite using oxygen isotope disequilibrium as was done previously in the PNM [*Buchwald and Casciotti*, 2013]. However, at high extents of nitrite oxidation (i.e., low $\delta^{15}N_{NO2}$), there is some evidence for O isotope equilibration because the measured $\delta^{18}O_{NO2}$ values (Figure 5b, gray symbols) are closer to equilibrium than $\delta^{18}O_{NO2,biotic}$ values (Figure 5b, open triangles). Using the methods described in *Buchwald and Casciotti* [2013], a residence time of ~98 ± 39 days is estimated for the most depleted $\delta^{15}N_{NO2}$ samples (−35‰ to −40‰). In this environment, it is not accurate to ignore the effects of nitrite reduction even on these samples with low $\delta^{15}N_{NO2}$ values; therefore, this residence time is probably an upper estimate (NO_2^- could be turning over more quickly). In order to resolve the importance of these possible nitrite sinks, we need to consider all available isotope tracers and nutrient concentrations.

4.2. SNM Nitrogen Cycling: 1-D Reaction Diffusion Model Setup

In order to integrate measurements of nitrite and nitrate concentration and isotope profiles into a more quantitative analysis of the relative rates of nitrate reduction, nitrite reduction, and nitrite oxidation, an isotope-enabled

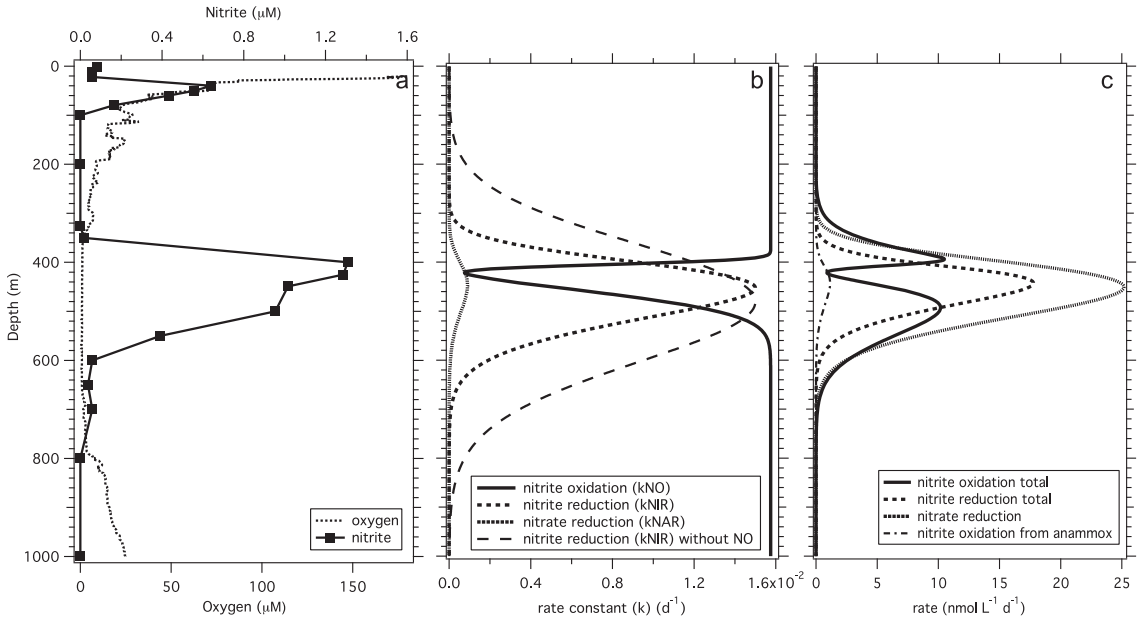

Figure 7. (a) The nitrite (filled squares) and oxygen (dashed line) concentration data from cycle 5, where the data constraining the model run were collected. (b) Profiles of the first order rate constants (d^{-1}) for nitrate reduction (k_{NAR}, dotted line), nitrite reduction (k_{NIR}, dashed line), and nitrite oxidation (k_{NXR}, solid line) used in model run five generating the best fit to data. Also shown (wide dashed line) is the k_{NIR} distribution in scenarios 2 and 3 where nitrite oxidation was excluded. (c) Profiles of the reaction rates ($\mu mol\ L^{-1}\ d^{-1}$), calculated from the nitrate or nitrite concentrations and rate constants for the best fit model (scenario 5). An estimate of nitrite oxidation from anammox, using the ratio of 0.28 of anammox to denitrification for nitrite reduction and then the ratio of 0.3 for nitrite reduction and nitrite oxidation from the stoichiometry of anammox is also shown in Figure 7c (dash-dotted line).

1-D biogeochemical model was constructed that can be used to understand the processes and rates needed to match the observed data. The model is a finite difference advection-diffusion-reaction model with ~1 h (0.05 day) time steps and 1 m depth resolution over 0–1000 m. The model included the physical processes of vertical advection (A) and diffusion (D), which could redistribute chemicals within the water column within, or into and out of, the ODZ. A ($0.016\ m\ yr^{-1}$) and D ($8.6\ m^2\ yr^{-1}$) values taken from *Anderson et al.* [1982] were similar to values measured and used in a previous model of the CRD [*Fiedler et al.*, 1991]. The sensitivity of the model to these physical parameters was low; even with a 10-fold change in each of the parameters, there was little change in model fit.

The biological processes that were represented in the oxygen deficient portion of the model (400–700 m) are shown in Figure 6. Within the ODZ, nitrite was produced by dissimilatory nitrate reduction and consumed by nitrite reduction (via anammox or denitrification) and nitrite oxidation (via nitrite-oxidizing bacteria (NOB) or anammox). Outside of the ODZ, nitrate reduction and nitrite reduction were assumed to be negligible, although nitrite oxidation was allowed to continue. The equations used to model the eight parameters, $^{14}NO_2^-$, $^{15}NO_2^-$, $N^{16}O_2^-$, $N^{18}O_2^-$, $^{14}NO_3^-$, $^{15}NO_3^-$, $N^{16}O_3^-$, and $N^{18}O_3^-$, are show in Appendix A.

The processes of nitrite oxidation, nitrite reduction, and nitrate reduction were considered first order processes with rate constants of k_{NXR}, k_{NAR}, and k_{NIR}, respectively, in units of d^{-1}. The rate constants for nitrate reduction (k_{NAR}) and nitrite reduction (k_{NIR}) were parameterized as skewed Gaussian distributions with depth within the ODZ, normalized to a maximum rate constant occurring at the peak of the nitrate deficit and SNM (Figure 7b). The exact depths of the maximum rate constants were determined based on the best fit to the observed concentration profiles, which resulted in a depth for k_{NAR} and k_{NIR} maxima of 405 m. The parameterization of k_{NIR} was different between the model runs with and without nitrite oxidation in order to fit the observed nitrite profile (Figure 7b). The nitrite oxidation rate constant (k_{NXR}) was modeled as an inverse skewed Gaussian distribution where it was highest everywhere outside the ODZ and had a minimum within the ODZ at a depth of 390 m (Figure 7b). These distributions of rates gave the best fit to the observed concentration and isotope profiles, rather than Gaussian distributions with no skew, and are consistent with a higher rate of organic matter input at the top of the ODZ to fuel heterotrophic nitrate reduction and nitrite reduction. Nitrite reduction by anammox bacteria might not be directly affected by organic matter input but

Table 1. Terms Used in the Secondary Nitrite Maximum 1-D Model

Process	Term	Value	References
Advection	A	0.016 m/d	*Anderson et al.* [1982]
Diffusion	D	8.6 m^2/d	*Anderson et al.* [1982]
Nitrite oxidation	$^{15}\alpha_{NXR}$	0.970	From model fit
	$^{18}\alpha_{NXR}$	0.997	*Buchwald and Casciotti* [2010]
	$^{18}\alpha_{H2O}$	1.010	*Buchwald and Casciotti* [2010]
Nitrate Reduction	$^{15}\alpha_{NAR}$	1.025	From model fit
	$^{18}\alpha_{NAR}$	1.025	From model fit; *Granger et al.* [2008]
	$^{18}\alpha_{b}$	0.975	*Casciotti and McIlvin* [2007]
Nitrite Reduction	$^{15}\alpha_{NIR}$	1.000	From model fit
	$^{18}\alpha_{NIR}$	1.000	From model fit
Abiotic Nitrite Exchange	$^{18}\alpha_{EXCH}$	1.013	*Casciotti et al.* [2007]

relies on provision of ammonium from organic matter degradation [*Ward*, 2013] or vertical migration of zooplankton [*Bianchi et al.*, 2014]. This model did not explicitly separate nitrite reduction or oxidation by anammox bacteria from denitrifying organisms and nitrite oxidizers, respectively. However, these contributions are considered later in the discussion using elemental [*Babbin et al.*, 2014] and biochemical [*Strous et al.*, 2006] stoichiometry for anammox. Here anammox was implicitly included in the flux estimates with isotope effects for nitrite reduction and nitrite oxidation [*Brunner et al.*, 2013] identical to heterotrophic denitrification [*Bryan et al.*, 1983] and nitrite oxidation by NOB [*Casciotti*, 2009; *Buchwald and Casciotti*, 2010], respectively.

In addition to the nitrite and nitrate concentrations, the distribution of the heavy isotopes (^{15}N and ^{18}O) was also modeled (Table 1 and Figure 6). The ^{15}N atoms were treated the same as the concentrations, except with each rate constant divided by a fractionation factor ($^{15}\alpha_{NXR}$, $^{15}\alpha_{NAR}$, and $^{15}\alpha_{NIR}$), which describes the ratio of rate constants for the light and heavy isotopes defined as $^{15}\alpha = {}^{14}k/{}^{15}k$, such that normal fractionation will be greater than 1 and inverse fractionation will be less than 1. The fractionation factor is related to an isotope effect by the equation: $\varepsilon\ (‰) = (\alpha - 1) \times 1000$, such that a normal isotope effect is positive and an inverse isotope effect is negative. In the case of nitrite oxidation, there is oxygen isotope fractionation ($^{18}\alpha_{NXR}$) during the selection of the nitrite molecule and also for the selection of a water molecule ($^{18}\alpha_{H2O}$) [*Buchwald and Casciotti*, 2010]. In nitrate reduction, there is oxygen isotope fractionation ($^{18}\alpha_{NAR}$) on the nitrate molecule [*Granger et al.*, 2008; *Kritee et al.*, 2012] as well as a branching isotope effect for the selection of which oxygen molecule is removed ($^{18}\alpha_{b}$) [*Casciotti et al.*, 2007]. Last, for the nitrite oxygen isotopes, we included a rate constant for abiotic exchange (k_{EXCH}) with an equilibrium fractionation factor that describes the unequal partitioning of ^{18}O between water and nitrite during this process ($^{18}\alpha_{EXCH}$). The model was used to optimize certain parameters that have broad ranges in the literature ($^{15}\alpha_{NXR}$, $^{15}\alpha_{NAR}$, $^{18}\alpha_{NAR}$, $^{15}\alpha_{NIR}$, and $^{18}\alpha_{NIR}$), while others we set at a constant value ($^{18}\alpha_{NXR}$, $^{18}\alpha_{H2O}$, $^{18}\alpha_{b}$, and k_{EXCH}). The values for these parameters used are shown in Table 1.

The model was initialized with nitrite concentrations set to zero throughout the profile and a nitrate profile typical for Pacific waters outside the ODZ (with minimal nitrate deficit). The model was run for 4 years, which is the average age of the water in the ETNP ODZ [*DeVries et al.*, 2012]. In order to illustrate the effects of nitrite oxidation, nitrite reduction, and oxygen atom exchange on the distributions of nitrate and nitrite concentrations and isotopes, five different model scenarios were analyzed (Figure 8). The first scenario included only nitrate reduction, tuning the k_{NAR} magnitude, and distribution to fit the nitrate concentration data. The second scenario included both nitrate and nitrite reduction, optimizing k_{NAR} and k_{NIR} to find the magnitude and distribution of these processes that best fit the nitrite concentration profile (Figure 7b). The third scenario added nitrite oxygen isotope exchange to scenario two. The last two scenarios included nitrite oxidation with and without oxygen isotope exchange.

To determine the distribution of rate constants and the fractionation factors most consistent with our data, a cost function (equation (1)) was used to evaluate the model and data agreement at a variety of maximum rate constants for all four processes (nitrite oxidation, nitrate reduction, nitrite reduction, and exchange; Figure 8, scenario five). The cost function is the sum of the squared differences between the data and model for the number of data points (N) and for each of the 6 variables ($i = [NO_2^-]$, $[NO_3^-]$, $\delta^{15}N_{NO2}$, $\delta^{18}O_{NO2}$, $\delta^{15}N_{NO3}$, and $\delta^{18}O_{NO3}$). The weight (W) represents a chosen weight for each variable so that even when

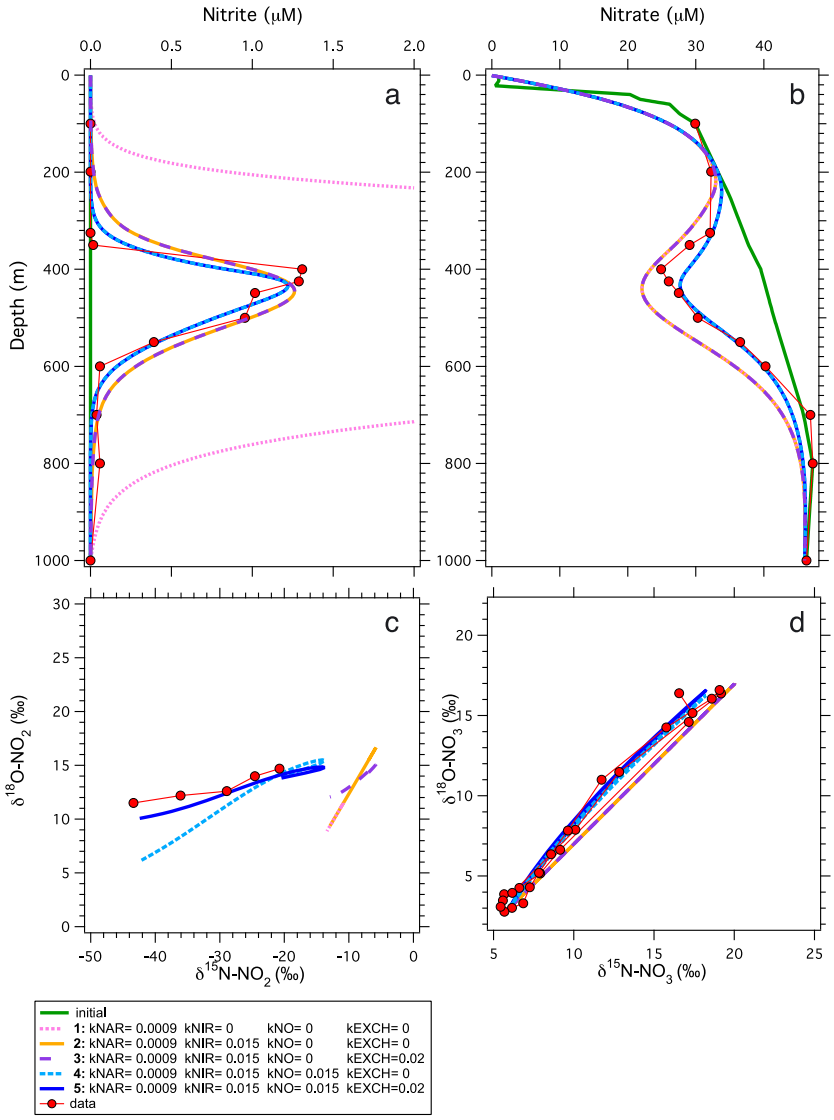

Figure 8. Depth profiles of (a) nitrite and (b) nitrate concentrations and dual isotope plots of (c) nitrite and (d) nitrate plotted for five different model runs with different rate parameterizations for nitrate reduction, nitrite reduction, nitrite oxidation, and oxygen atom exchange, described in the text. The data shown (red symbols in each panel) are from cycle 5.

the absolute values are smaller they had equal weighting in the cost. The weights were determined by using the mean of the data points, and some were adjusted by a factor of 10 until each of the variables all had approximately equal costs.

$$\text{cost} = \sqrt{\sum_{i=1}^{6}\sum_{j=1}^{N}\frac{\left(x_i - x_i^{\text{obs}}\right)^2}{NW}} \tag{1}$$

4.3. SNM Nitrogen Cycling: 1-D Reaction Diffusion Model Results

In the first of the five scenarios (1) (Figure 8, dotted pink lines), we allowed only nitrate reduction to occur, with no consumption of nitrite. In order to obtain the correct nitrate deficit (Figure 8b), the maximum rate constant for nitrate reduction (k_{NAR}) was set to 0.0009 d^{-1}, corresponding to a maximum rate of nitrate reduction near 25 nmol L^{-1} d^{-1} (Figure 7c) and an ODZ-integrated nitrate reduction rate of 3.7 mmol N m^{-2} d^{-1}. With this rate of nitrate reduction and no nitrite sinks, this scenario predictably overestimated the nitrite concentration in the SNM, which increased to over 15 μM (off scale in Figure 8a). In the second scenario (2)

(Figure 8, solid orange lines), nitrite reduction was added as a sink of nitrite, with its magnitude adjusted until the level of nitrite accumulation matched the observed profile. For this scenario, nitrite reduction was forced to occur outside of the ODZ to match the distribution of nitrite in the water column (Figure 7b, dashed line).

The modeled relationship of $\delta^{15}N_{NO2}$ and $\delta^{18}O_{NO2}$ in scenarios 1 and 2 had a much higher slope than our data (Figure 8c), with a higher than observed range of $\delta^{15}N_{NO2}$ values. In the third scenario (3) (dashed purple line), the added exchange of oxygen atoms between nitrite and water ($k_{EXCH} = 0.02$) lowered the slope of $\delta^{18}O_{NO2}$ versus $\delta^{15}N_{NO2}$ to be consistent with the data (Figure 8c), although the modeled $\delta^{15}N_{NO2}$ values remained too high. In these first three scenarios, where there was no nitrite oxidation, the $\delta^{15}N_{NO3}$ and $\delta^{18}O_{NO3}$ values followed a 1:1 line originating at deepwater nitrate $\delta^{15}N_{NO3}$ and $\delta^{18}O_{NO3}$ values. This is expected because the N and O isotope effects for nitrate reduction are equal, and nitrite reduction does not directly affect $\delta^{15}N_{NO3}$ or $\delta^{18}O_{NO3}$. This constant ratio of increases in $\delta^{15}N_{NO3}$ and $\delta^{18}O_{NO3}$ does not match observed nitrate isotope variations, which tended to fall above this 1:1 line (Figure 8d), reflecting negative $\Delta(15,18)$ values. The $\delta^{15}N_{NO2}$ values predicted in these first three scenarios are also too high. The only mechanisms to lower $\delta^{15}N_{NO2}$ values without nitrite oxidation are to increase the isotope effect for nitrate reduction ($^{15}\alpha_{NAR}$) and/or decrease the isotope effect for nitrite reduction ($^{15}\alpha_{NIR}$). However, increased $^{15}\alpha_{NAR}$ leads to a poorer fit to observed $\delta^{15}N_{NO3}$ values (not shown), and $^{15}\alpha_{NIR}$ is already set to 1.000, its lowest possible value.

Nitrite oxidation was added to the model in the fourth (4) (light blue dashed line) and fifth (5) (dark blue solid line) scenarios, which allowed the data to be more closely simulated. Here the modeled $\delta^{15}N_{NO3}$ and $\delta^{18}O_{NO3}$ values yielded the negative $\Delta(15,18)$ values observed (Figure 8d). Also, the $\delta^{15}N_{NO2}$ values were lowered significantly by the fractionation during nitrite oxidation to values encompassing those observed. Allowing oxygen atom exchange (scenario 5) more accurately simulated the range and pattern of observed $\delta^{18}O_{NO2}$ values than the scenario without oxygen atom exchange (scenario 4). Therefore, oxygen isotope exchange is required to explain $\delta^{18}O_{NO2}$ data, as suggested in section 4.1. Furthermore, allowing nitrite oxidation to occur within and on the fringes of the ODZ improved the data-model comparison for nitrite concentration and the distributions of nitrate and nitrite isotopes. Clearly not all nitrite consumption can be explained by nitrite oxidation, as the fact that a DIN deficit is present requires nitrite reduction to have occurred. We find that by combining nitrite oxidation in the upper and lower portions of the ODZ with nitrite reduction in the center (Figure 7c), we have the best fit to all the data (dark blue lines in Figure 8). Rates of nitrite oxidation and nitrite reduction required to best fit the concentration and isotopic data peaked at 10 nM d^{-1} and 15 nM d^{-1}, respectively, and both gave depth-integrated fluxes between 200 and 1000 m of 1.8 mmol m^{-2} d^{-1}, meaning nitrite oxidation was responsible for 50% of nitrite consumption in and around the SNM. These fluxes give a steady state residence time for nitrite in the SNM around 100 days, when assuming only nitrite oxidation as a sink, similar to that obtained using the $\delta^{18}O_{NO2}$ disequilibrium approach described above.

Although anammox is not explicitly included in the model, the ratios of nitrite oxidation and nitrite reduction that best fit the isotopic data can be used to constrain the contributions of anammox to nitrite oxidation and nitrite reduction in the ODZ. During the process of anammox there is a portion of nitrite that is oxidized and a portion that is reduced to N_2 gas; the expected ratio for nitrite oxidation to nitrite reduction during anammox is 0.3 [*Brunner et al.*, 2013; *Strous et al.*, 2006]. We used this ratio in combination with modeled nitrite reduction rates to estimate the contribution of anammox to nitrite oxidation in the ODZ, assuming that anammox contributes 28% of nitrite reduction [*Babbin et al.*, 2014; *Dalsgaard et al.*, 2012]. At the peak of the SNM, anammox can account for all of the required nitrite oxidation, at a rate near 2 nM d^{-1} (Figure 7c). However, outside of this narrow zone, much more nitrite oxidation is required than can be attributed to anammox. Overall, anammox contributes 0.12 mmol m^{-2} d^{-1} to the total nitrite oxidation flux of 1.8 mmol m^{-2} d^{-1} or 7% of the required nitrite oxidation. Even if all of the nitrite reduction were carried out by anammox, the amount of nitrite oxidation predicted by the model exceeds what would be derived by anammox. Unless the stoichiometry of nitrite reduction and nitrite oxidation by anammox is flexible, there appears to be a role for nitrite-oxidizing bacteria in the ODZ. The main conclusion that can be drawn from this exercise about the relative roles of anammox and denitrification in nitrite reduction is that the required nitrite oxidation rates at the SNM peak (near the peak in nitrite reduction rates) are consistent with anammox contributing 28% and denitrification contributing 72% to nitrite reduction.

The fractionation factors that were predicted from the model often agreed with previous studies, but there were some discrepancies. The $^{15}\alpha_{NAR}$ and $^{18}\alpha_{NAR}$ were predicted to be 1.025, which is consistent with previous experimental and field studies [*Granger et al.*, 2008; *Casciotti et al.*, 2013; *Kritee et al.*, 2012; *Bourbonnais et al.*, 2015]. The $^{15}\alpha_{NXR}$ was predicted to be 0.970, which is similar to that found in anammox [*Brunner et al.*, 2013] but larger than measured in laboratory cultures of nitrite-oxidizing bacteria (NOB) [*Casciotti*, 2009; *Buchwald and Casciotti*, 2010]. This level of isotopic fractionation during nitrite oxidation was also required to explain nitrate and nitrite isotope distributions in the eastern tropical South Pacific (ETSP) [*Casciotti et al.*, 2013]. The fractionation factors for nitrite reduction that best fit the data was 1.00, indicating no fractionation. Again this is consistent with previous modeling efforts but has a significant discrepancy from measurements in anammox bacteria [*Brunner et al.*, 2013] and ODZ field measurements [*Bourbonnais et al.*, 2015].

4.4. SNM Nitrogen Cycling: Combining Isotope Profiles, Rate Incubations, and Molecular Data

The model predicts a maximum nitrate reduction rate of 25 nM d^{-1}, maximum nitrite reduction rate of 15 nM d^{-1}, and nitrite oxidation of 10 nM d^{-1} (Figure 7c), with integrated rates of nitrite reduction and oxidation balancing each other. These rates represent space- and time-averaged rates of the biogeochemical processes over their residence time in the ODZ and may not be expected to reflect the rates observed in instantaneous rate measurements. The nitrate reduction rates derived from the model are similar to geochemical estimates from the Arabian Sea [*Devol et al.*, 2006] and the ETSP [*Casciotti et al.*, 2013] and in the middle of instantaneous measurements of nitrate reduction in the eastern tropical Pacific [*Codispoti and Christensen*, 1985; *Kalvelage et al.*, 2013; *Dalsgaard et al.*, 2012]. Nitrite reduction rates predicted by the model are also in line with rate measurements of nitrite reduction from anammox and denitrification in the Arabian Sea (1.8 to 36 nM d^{-1}) [*Jensen et al.*, 2011].

The nitrite oxidation rates predicted from the model are uniformly lower than those measured in the Nambian ODZ ($\leq$372 nM d^{-1}) [*Füssel et al.*, 2012], the eastern tropical North Pacific (63.7–213 nM d^{-1}) [*Beman et al.*, 2013; *Ganesh et al.*, 2015], and the eastern tropical South Pacific (170–600 nM d^{-1}) [*Lipschultz et al.*, 1990], but on par with other geochemical estimates in the South Pacific [*Casciotti et al.*, 2013]. The presence of nitrite oxidation in suboxic waters is still puzzling despite evidence from instantaneous rate measurements, the presence of nitrite oxidizing bacteria [*Füssel et al.*, 2012; *Beman et al.*, 2013; *Ganesh et al.*, 2015, this study], and stable isotopic signatures of nitrite oxidation [*Casciotti*, 2009; *Casciotti et al.*, 2013; *Gaye et al.*, 2013; *Bourbonnais et al.*, 2015, this study]. This suggests that nitrite-oxidizing bacteria can utilize oxygen at very low concentrations or that they utilize alternate electron acceptors for oxidizing nitrite to nitrate. The use of episodically injected O_2 is also a possibility, although competition with heterotrophic bacteria for this source of O_2 could be prohibitive.

Our instantaneous ammonia oxidation rates (maximum ~3 nM d^{-1}) were similar to those measured in the Arabian Sea (3.6 $\pm$ 0.04 nM d^{-1}) [*Lam et al.*, 2011] and the ETNP ($<$5 nM d^{-1}) [*Beman et al.*, 2013] but lower than those detected in the Peruvian ODZ (77–144 nM d^{-1}) [*Lam et al.*, 2009]. The archaeal *amoA* abundances measured here (0 to 5236 copies mL^{-1}) were also lower than previous studies in the Peruvian ODZ [*Lam et al.*, 2009] but similar to measurements in the Arabian Sean [*Lam et al.*, 2011]. It is interesting to note that the measured ammonia oxidation rates are considerably lower than the nitrite oxidation rates estimated from our 1-D model (~10 nM d^{-1}). Here nitrate reduction is likely to be a more significant source of nitrite to NOB than is ammonia oxidation, providing a mechanism for decoupling the two steps of nitrification that are classically thought to be tightly linked. This finding parallels the N cycle observed in the Namibian ODZ [*Füssel et al.*, 2012].

The detection of *Nitrospina*-like NOB from qPCR data within the ODZ above and below the SNM follows the inferred distribution of nitrite oxidation rates from the 1-D model. In previous studies where *amoA* and *Nitrospina* 16S rRNA gene copies were measured in the same profiles, archaeal *amoA* genes were about 4 times more abundant than *Nitrospina* 16S rRNA [*Mincer et al.*, 2007; *Santoro et al.*, 2010]. These studies were in Monterey Bay and the California Current, both upwelling systems with high productivity and higher total abundances of archaeal *amoA*. The observation of higher relative abundances of *Nitrospina* here is unique and possibly linked to the source of nitrite from nitrate reduction in the ODZ. *Nitrospina* has also been detected in the Namibian ODZ [*Füssel et al.*, 2012], ETNP [*Beman et al.*, 2013], and ETSP [*Levipan et al.*, 2014] at abundances up to 10 times higher than those found here. The data from these other ODZs coupled with our data suggest that an active cycle of nitrate reduction coupled to nitrite reoxidation may select for higher abundances of NOB relative to ammonia-oxidizing organisms. Indeed, the high abundance of NOB compared to AOA and AOB seems to suggest that NOB could be operating independently of AOA and AOB in oxygen deficient environments. Additional genera of NOB not quantified here, such as *Nitrococcus*,

may also be important in ODZs [*Füssel et al.*, 2012]. The inclusion of these taxa, however, would only serve to further increase the relative abundance of NOB.

5. Conclusions

The major finding from the current study is that about 50% of the nitrate that is reduced to nitrite is reoxidized back to nitrate rather than being reduced further to N_2, with some of the oxidation being predicted within the ODZ. Multiple isotope tracers including $\delta^{15}N_{NO2}$, $\delta^{18}O_{NO2}$, $\delta^{15}N_{NO3}$, $\delta^{18}O_{NO3}$, and their derivatives Δ(15,18) and $\Delta\delta^{15}N$, along with concentration measurements of nitrite, nitrate, ammonium, and oxygen, were found to be powerful tools in interpreting nitrogen cycling in the SNM of the eastern tropical North Pacific Ocean within the Costa Rica Upwelling Dome. Nitrate concentration and isotope profiles suggested a nitrate sink by dissimilatory nitrate reduction, based on enrichment of $\delta^{15}N_{NO3}$ and $\delta^{18}O_{NO3}$. The nitrite isotopes, Δ(15,18) and $\Delta\delta^{15}N$, also revealed a strong influence of nitrite reoxidation in the SNM. Our analysis agrees with the other recent studies suggesting that nitrite reoxidation is an important process in and around ODZs [*Füssel et al.*, 2012; *Casciotti et al.*, 2013; *Beman et al.*, 2013; *Levipan et al.*, 2014; *Ganesh et al.*, 2015]. Our rates and distributions of nitrite oxidation and nitrite reduction are also within the range of what *Anderson et al.* [1982] predicted and close to what *Casciotti* [2009] estimated for the ETNP. The interpretation that the negative deviations in Δ(15,18) can be caused by nitrite reoxidation also matches the interpretation of nitrate isotopes in the ETNP by *Sigman et al.* [2005] and *Casciotti and McIlvin* [2007]. Here we have added to the mounting evidence of nitrite oxidation within anoxic regions, which has implications for the control of N loss in ODZs and the carbon cycle in that the reoxidation of nitrite retains fixed N in a bioavailable form for primary producers and provides nitrate for further heterotrophic respiration. While NOB in the *Nitrospina* lineage are autotrophic microorganisms [*Lücker et al.*, 2013], the amount of carbon fixed by these organisms into organic matter is small in comparison to the degradation of organic matter that could occur through heterotrophic nitrate reduction. Also, while there is still no mechanistic explanation for the activity of NOB under oxygen deficiency, the activity and controls on nitrite oxidation in the ODZ is an important area of future research that will help better predict the fate of the marine N budget under enhanced ocean stratification and deoxygenation.

Appendix A

A1. Equations Used in the 1-D Reaction Diffusion Model

The model used is a one-dimensional (1-D) model that iterates over time (t) and depth (z). The time step (Δt) used was 0.05 days, which is then run for 29,200 time steps or 4 years. The domain is set at 1000 m and each bin (Δz) is set at 1 m. Equations (A1)–(A8) represent the eight different parameters ($^{14}NO_2^-$, $^{15}NO_2^-$, $N^{16}O_2^-$, $N^{18}O_2^-$, $^{14}NO_3^-$, $^{15}NO_3^-$, $N^{16}O_3^-$, and $N^{18}O_3^-$). Each parameter is transported by advection ($A = 6\,m\,yr^{-1}$) and diffusion ($D = 3000\,m^2\,yr^{-1}$) and is subject to biogeochemical processes of nitrate reduction (NAR), nitrite reduction (NIR), and nitrite oxidation (NXR). The first order rates of nitrate reduction (k_{NAR}), nitrite reduction (k_{NIR}), nitrite oxidation (k_{NXR}) and the fractionation factors in N for those three processes ($^{15}\alpha_{NAR}$, $^{15}\alpha_{NIR}$, and $^{15}\alpha_{NO}$), and the fractionation factors associated with O ($^{18}\alpha_{NAR}$, $^{18}\alpha_{NAR}$, $^{18}\alpha_{NO}$, $^{18}\alpha_{EXCH}$, $^{18}\alpha_b$, and $^{18}\alpha_{H2O}$) are taken from the literature or fit by the model. The $^{18}\alpha_{EXCH}$ is the equilibrium fractionation factor for the abiotic exchange of oxygen atoms between water and nitrite, $^{18}\alpha_b$ is the branching fractionation or kinetic isotope fractionation during the removal of the oxygen atom from nitrate during nitrate reduction, and $^{18}\alpha_{H2O}$ is the fractionation factor for the oxygen incorporation from water during nitrite oxidation. The isotopic composition of the water ($\delta^{18}O_{H2O}$) is set to 0‰ and the $^{18}O/^{16}O$ ratio for the standard Vienna Mean Ocean Water ($^{18}R_{VSMOW}$). The values used for k values are shown in Figure 7b and Figure 8. The values used for the isotope fractionation factors are shown in Table 1.

$$
\begin{aligned}
&{}^{14}NO_2^-(iZ, iT+1) = {}^{14}NO_2^-(iZ, iT) + \Delta t \times (\ldots \\
&D(iZ) \times \left({}^{14}N^{16}O_2^-(iZ+1, iT) - 2 \times {}^{14}NO_2^-(iZ, iT) + {}^{14}NO_2^-(iZ-1, iT)\right)/\Delta z^2 + \ldots \\
&A \times ({}^{14}NO_2^-(iZ+1, iT) - {}^{14}NO_2^-(iZ-1, iT))/2/\Delta z - \ldots \\
&k_{NXR}(iZ) \times {}^{14}NO_2^-(iZ, iT) + \ldots \\
&k_{NAR}(iZ) \times {}^{14}NO_3^-(iZ, iT) - \ldots \\
&k_{NIR}(iZ) \times {}^{14}NO_2^-(iZ, iT))
\end{aligned}
\tag{A1}
$$

$$
\begin{aligned}
&{}^{15}NO_2^-(iZ,iT+1) = {}^{15}NO_2^-(iZ,iT) + \Delta t\times(\ldots\\
&D(iZ)\times({}^{15}NO_2^-(iZ+1,iT) - 2\times{}^{15}NO_2^-(iZ,iT) + {}^{15}NO_2^-(iZ-1,iT))/\Delta z^2 + \ldots\\
&A\times({}^{15}NO_2^-(iZ+1,iT) - {}^{15}NO_2^-(iZ-1,iT))/2/\Delta z - \ldots\\
&k_{NXR}(iZ)/{}^{15}\alpha_{NXR}\times{}^{15}NO_2^-(iZ,iT) + \ldots\\
&k_{NAR}(iZ)/{}^{15}\alpha_{NAR}\times{}^{15}NO_3^-(iZ,iT) - \ldots\\
&k_{NIR}(iZ)/{}^{15}\alpha_{NIR}\times{}^{15}NO_2^-(iZ,iT));
\end{aligned}
\tag{A2}
$$

$$
\begin{aligned}
&N^{16}O_2^-(iZ,iT+1) = N^{16}O_2^-(iZ,iT) + \Delta t\times(\ldots\\
&D(iZ)\times\left(N^{16}O_2^-(iZ+1,iT) - 2\times N^{16}O_2^-(iZ,iT) + N^{16}O_2^-(iZ-1,iT)\right)/\Delta z^2 + \ldots\\
&k_{NXR}(iZ)\times 2\times{}^{14}NO_2^-(iZ,iT) + \ldots\\
&k_{NAR}(iZ)\times 2\times{}^{14}NO_3^-(iZ,iT) - \ldots\\
&k_{NIR}(iZ)\times 2\times{}^{14}NO_2^-(iZ,iT));
\end{aligned}
\tag{A3}
$$

$$
\begin{aligned}
&N^{18}O_2^-(iZ,iT+1) = N^{18}O_2^-(iZ,iT) + \Delta t\times(\ldots\\
&D(iZ)\times\left(N^{18}O_2^-(iZ+1,iT) - 2\times N^{18}O_2^-(iZ,iT) + N^{18}O_2^-(iZ-1,iT)\right)/\Delta z^2 + \ldots\\
&A\times\left(N^{18}O_2^-(iZ+1,iT) - N^{18}O_2^-(iZ-1,iT)\right)/2/\Delta z - \ldots\\
&k_{NXR}(iZ)/{}^{18}\alpha_{NXR}\times\ N^{18}O_2^-(iZ,iT) + \ldots\\
&k_{NAR}(iZ)/{}^{18}\alpha_{NAR}/{}^{18}\alpha_{branching}\times 2/3\times N^{18}O_3^-(iZ,iT) - \ldots\\
&k_{NIR}(iZ)/{}^{18}\alpha_{NIR}\times N^{18}O_2^-(iZ,iT) - \ldots\\
&k_{EXCH}(iZ)\times N^{18}O_2^-(iZ,iT) + \ldots\\
&k_{EXCH}(iZ)\times N^{16}O_2^-(iZ,iT)\times{}^{18}\alpha_{EXCH}\times\left(\delta^{18}O_{H2O}/1000+1\right)\times{}^{18}R_{VSMOW});
\end{aligned}
\tag{A4}
$$

$$
\begin{aligned}
&{}^{14}NO_3^-(iZ,iT+1) = {}^{14}NO_3^-(iZ,iT) + \Delta t\times(\ldots\\
&D(iZ)\times({}^{14}NO_3^-(iZ+1,iT) - 2\times{}^{14}NO_3^-(iZ,iT) + {}^{14}NO_3^-(iZ-1,iT))/\Delta z^2 + \ldots\\
&A\times({}^{14}NO_3^-(iZ+1,iT) - {}^{14}NO_3^-(iZ-1,iT))/2/\Delta z + \ldots\\
&k_{NXR}(iZ)\times{}^{14}NO_2^-(iZ,iT) - \ldots\\
&k_{NAR}(iZ)\times{}^{14}NO_3^-(iZ,iT));
\end{aligned}
\tag{A5}
$$

$$
\begin{aligned}
&{}^{15}NO_3^-(iZ,iT+1) = {}^{15}NO_3^-(iZ,iT) + \Delta t\times(\ldots\\
&D(iZ)\times({}^{15}NO_3^-(iZ+1,iT) - 2\times{}^{15}NO_3^-(iZ,iT) + {}^{15}NO_3^-(iZ-1,iT))/\Delta z^2 + \ldots\\
&A\times({}^{15}NO_3^-(iZ+1,iT) - {}^{15}NO_3^-(iZ-1,iT))/2/\Delta z + \ldots\\
&k_{NXR}(iZ)/{}^{15}\alpha_{NXR}\times{}^{15}NO_2^-(iZ,iT) - \ldots\\
&k_{NAR}(iZ)/{}^{15}\alpha_{NAR}\times{}^{15}NO_3^-(iZ,iT));
\end{aligned}
\tag{A6}
$$

$$
\begin{aligned}
&N^{16}O_3^-(iZ,iT+1) = N^{16}O_3^-(iZ,iT) + dt\times(\ldots\\
&D(iZ)\times\left(N^{16}O_3^-(iZ+1,iT) - 2\times N^{16}O_3^-(iZ,iT) + N^{16}O_3^-(iZ-1,iT)\right)/\Delta z^2 + \ldots\\
&A\times\left(N^{16}O_3^-(iZ+1,iT) - N^{16}O_3^-(iZ-1,iT)\right)/2/\Delta z + \ldots\\
&3\times k_{NXR}(iZ)\times{}^{14}NO_2^-(iZ,iT) - \ldots\\
&k_{NAR}(iZ)\times 3\times{}^{14}NO_3^-(iZ,iT));
\end{aligned}
\tag{A7}
$$

$$
\begin{aligned}
&N^{18}O_3^-(iZ,iT+1) = N^{18}O_3^-(iZ,iT) + \Delta t\times(\ldots\\
&D(iZ)\times\left(N^{18}O_3^-(iZ+1,iT) - 2\times N^{18}O_3^-(iZ,iT) + N^{18}O_3^-(iZ-1,iT)\right)/\Delta z^2 + \ldots\\
&A\times\left(N^{18}O_3^-(iZ+1,iT) - N^{18}O_3^-(iZ-1,iT)\right)/2/\Delta z + \ldots\\
&k_{NXR}(iZ)/{}^{18}\alpha_{NXR}\times\ N^{18}O_2^-(iZ,iT) + \ldots\\
&k_{NXR}(iZ)/{}^{18}\alpha_{H2O}\times{}^{14}NO_2^-(iZ,iT)\times\left(\delta^{18}O_{H2O}/1000+1\right)\times{}^{18}R_{VSMOW}) - \ldots\\
&k_{NAR}(iZ)/{}^{18}\alpha_{NAR}\times N^{18}O_3^-(iZ,iT));
\end{aligned}
\tag{A8}
$$

Acknowledgments
We are grateful to Mike Landry (Chief Scientist) and the Captain and crew of the R/V *Melville* for enabling the collection of the samples. We thank James Moffett and Dreux Chappell, participants on the cruise, for useful discussion and insight on the CRD. Also we thank Jessica Tsay for helping measure [NO_2^-] and Matt McIlvin for help analyzing isotope samples. We would like to thank Jeffrey Kaeli for his help in construction of the 1-D model. This research was funded by the National Science Foundation grants OCE 05-26277, OCE 09-610998 to KLC, and a WHOI Coastal Ocean Institute award to CB. Data are provided within the figures and tables and have been submitted to the Biological and Chemical Oceanography Data Management Office (www.bco-dmo.org).

References

Anderson, J. J., A. Okubo, A. S. Robbins, and F. A. Richards (1982), A model for nitrite and nitrate distributions in oceanic oxygen minimum zones, *Deep Sea Res., Part A*, *29*, 1113–1140, doi:10.1016/0198-0149(82)90031-0.

Babbin, A., R. G. Keil, A. H. Devol, and B. B. Ward (2014), Organic matter stoichiometry, flux, and oxygen control nitrogen loss in the ocean, *Science*, *344*, 406–408, doi:10.1126/science.1248364.

Babbin, A. R., D. Bianchi, A. Jayakumar, and B. B. Ward (2015) Rapid nitrous oxide cycling in the suboxic ocean, *Science*, *348*, 1127–1129, doi:10.1126/science.aaa8380.

Beman, J., J. L. Shih, and B. Popp (2013), Nitrite oxidation in the upper water column and oxygen minimum zone of the eastern tropical North Pacific Ocean, *ISME J.*, *7*, 2192–2205, doi:10.1038/ismej.2013.96.

Bianchi, D., A. R. Babbin, and E. E. Galbraith (2014), Enhancement of anammox by the excretion of diel vertical migrators, *Proc. Natl. Acad. Sci. U.S.A.*, *44*, 15,653–15,658, doi:10.1073/pnas.1410790111.

Bohlke, J. K., S. J. Mroczkowski, and T. B. Coplen (2003), Oxygen isotopes in nitrate: New reference materials for ^{18}O: ^{17}O: ^{16}O measurements and observations on nitrate-water equilibration, *Rapid Commun. Mass Spectrom.*, *17*, 1835–1846, doi:10.1002/rcm.1123.

Bourbonnais, A., M. A. Altabet, C. N. Charoenpong, J. Larkum, H. Hu, H. W. Bange, and L. Stramma (2015), N-loss isotope effects in the Peru oxygen minimum zone studied using a mesoscale eddy as a natural tracer experiment, *Global Biogeochem. Cycles*, *29*, 793–811, doi:10.1002/2014GB005001.

Brandes, J. A., and A. H. Devol (2002), A global marine-fixed nitrogen isotopic budget: Implications for Holocene nitrogen cycling, *Global Biogeochem. Cycles*, *16*(4), 1120, doi:10.1029/2001GB001856.

Brandhorst, W. (1959), Nitrification and denitrification in the Eastern tropical North Pacific, *J. Cons. Int. Explor. Mer.*, *25*, 2–20.

Broenkow, W. W. (1965), The distribution of nutrients in the Costa Rica Dome in the eastern tropical Pacific Ocean, *Limnol. Oceanogr.*, *10*, 40–52.

Brunner, B., et al. (2013), Nitrogen isotope effects induced by anammox bacteria, *Proc. Natl. Acad. Sci. U.S.A.*, *110*, 18,994–18,999, doi:10.1073/pnas.1310488110.

Bryan, B., G. Shearer, J. Skeeters, and D. Kohl (1983), Variable expression of the nitrogen isotope effect associated with denitrification of nitrite, *J. Biol. Chem.*, *258*, 8613–8617.

Buchwald, C., and K. L. Casciotti (2010), Oxygen isotopic fractionation and exchange during bacterial nitrite oxidation, *Limnol. Oceanogr.*, *55*, 1064–1074, doi:10.4319/lo.2010.55.3.1064.

Buchwald, C., and K. L. Casciotti (2013), Isotopic ratios of nitrite as tracers of the sources and age of oceanic nitrite, *Nat. Geosci.*, *4*, 308–313, doi:10.1038/ngeo1745.

Buchwald, C., A. E. Santoro, M. R. McIlvin, and K. L. Casciotti (2012), Oxygen isotopic composition of nitrate and nitrite produced by nitrifying cocultures in and natural marine assemblages, *Limnol. Oceanogr.*, *57*, 1361–1375, doi:10.4319/lo.2012.57.5.1361.

Casciotti, K. L. (2009), Inverse kinetic isotope fractionation during bacterial nitrite oxidation, *Geochim. Cosmochim. Acta*, *73*, 2061–2076, doi:10.1016/j.gca.2008.12.022.

Casciotti, K. L., and M. R. McIlvin (2007), Isotopic analyses of nitrate and nitrite from reference mixtures and application to eastern tropical North Pacific waters, *Mar. Chem.*, *107*, 184–201, doi:10.1016/j.marchem.2007.06.021.

Casciotti, K. L., D. M. Sigman, M. G. Hastings, J. K. Bohlke, and A. Hilkert (2002), Measurement of the oxygen isotopic composition of nitrate in seawater and freshwater using the denitrifier method, *Anal. Chem.*, *74*, 4905–4912, doi:10.1021/ac020113w.

Casciotti, K. L., J. K. Boehlke, M. R. McIlvin, S. J. Mroczkowski, and J. E. Hannon (2007), Oxygen isotopes in nitrite: Analysis, calibration, and equilibration, *Anal. Chem.*, *79*, 2427–2436, doi:10.1021/ac061598h.

Casciotti, K. L., C. Buchwald, and M. R. McIlvin (2013), Implications of nitrate and nitrite isotopic measurements for the mechanisms of nitrogen cycling in the Peru oxygen deficient zone, *Deep Sea Res., Part I*, *80*, 78–93, doi:10.1016/j.dsr.2013.05.017.

Christensen, J., J. Murray, A. Devol, and L. Codispoti (1987), Denitrification in the continental shelf sediments has a major impact on the oceanic nitrogen budget, *Global Biogeochem. Cycles*, *1*, 97–116, doi:10.1029/GB001i002p00097.

Codispoti, L. A. (1986), High nitrite levels off Northern Peru: A signal of instability in the marine denitrification rate, *Science*, *4769*, 1200–1202, doi:10.1126/science.233.4769.1200.

Codispoti, L. A., and J. P. Christensen (1985), Nitrification, denitrification and nitrous-oxide cycling in the Eastern Tropical South-Pacific Ocean, *Mar. Chem.*, *4*, 277–300, doi:10.1016/0304-4203(85)90051-9.

Codispoti, L. A., J. A. Brandes, J. P. Christensen, A. H. Devol, S. W. A. Naqvi, H. W. Paerl, and T. Yoshinari (2001), The oceanic fixed nitrogen and nitrous oxide budgets: Moving targets as we enter the anthropocene?, *Sci. Mar.*, *65*, 85–105.

Collos, Y. (1998), Nitrate uptake, nitrite release and uptake and new production estimates, *Mar. Ecol. Prog. Ser.*, *171*, 293–301, doi:10.3354/meps171293.

Dalsgaard, T., D. Canfield, J. Peterson, B. Thamdrup, and J. Acuña-González (2003), N_2 production by the anammox reaction in the anoxic water column of Golfo Dulce, Costa Rica, *Nature*, *422*, 606–608, doi:10.1038/nature01526.

Dalsgaard, T., B. Thamdrup, L. Farias, and N. P. Revsbech (2012), Anammox and denitrification in the oxygen minimum zone of the eastern South Pacific, *Limnol. Oceanogr.*, *57*, 1331–1346, doi:10.4319/lo.2012.57.5.1331.

Dalsgaard, T., A. H. Devol, B. B. Ward, O. Ulloa, D. E. Canfield, and N. P. Revsbech (2014), Oxygen distribution and aerobic respiration in the north and south eastern tropical Pacific oxygen minimum zones, *Deep Sea Res., Part I*, *94*, 173–183.

Deutsch, C., D. M. Sigman, R. C. Thunell, A. N. Meckler, and G. H. Haug (2004), Isotopic constraints on glacial/interglacial changes in the oceanic nitrogen budget, *Global Biogeochem. Cycles*, *18*, GB4012, doi:10.1029/2003GB002189.

Devol, A. H. (1991), Direct measurements of nitrogen gas fluxes from continental-shelf sediments, *Nature*, *349*, 319–321, doi:10.1038/349319a0.

Devol, A. H., A. G. Uhlenhopp, S. W. A. Naqvi, J. A. Brandes, D. A. Jayakumar, H. Naik, S. Gaurin, L. A. Codispoti, and T. Yoshinari (2006), Denitrification rates and excess nitrogen gas concentrations in the Arabian Sea oxygen deficient zone, *Deep Sea Res., Part I*, *9*, 1533–1547, doi:10.1016/j.dsr.2006.07.005.

DeVries, T., C. Deutsch, F. Primeau, B. Chang, and A. Devol (2012), Global rates of water-column denitrification derived from nitrogen gas measurements, *Nat. Geosci.*, *8*, 547–550, doi:10.1038/NGEO1515.

DeVries, T., C. Deutsch, P. A. Rafter, and F. Primeau (2013), Marine denitrification rates determined from a global 3-D inverse model, *Biogeosciences*, *4*, 2481–2496, doi:10.5194/bg-10-2481-2013.

Dore, J., and D. Karl (1996), Nitrification in the euphotic zone as a source of nitrite, nitrate and nitrous oxide at Station ALOHA, *Limnol. Oceanogr.*, *41*, 1619–1628.

Eppley, R. W., and B. J. Peterson (1979), Particulate organic-matter flux and planktonic new production in the deep ocean, *Nature*, *5740*, 677–680, doi:10.1038/282677a0.

Eugster, O., and N. Gruber (2012), A probablistic estimate of global marine N-fixation and denitrification, *Global Biogeochem. Cycles*, *26*, GB4013, doi:10.1029/2012GB004300.
Farias, L., C. Fernandez, J. Faundez, M. Cornejo, and M. E. Alcaman (2009), Chemolithoautotrophic production mediating the cycling of greenhouse gases N_2O and CH_4 in an upwelling ecosystem, *Biogeosciences*, *6*, 3053–3069, doi:10.5194/bg-6-3053-2009.
Fiedler, P. C., V. Philbrick, and F. P. Chavez (1991), Oceanic upwelling and productivity in the eastern tropical Pacific, *Limnol. Oceanogr.*, *8*, 1834–1850.
Francis, C. A., K. J. Roberts, J. M. Beman, A. E. Santoro, and B. B. Oakley (2005), Ubiquity and diversity of ammonia-oxidizing archaea in water columns and sediments of the ocean, *Proc. Natl. Acad. Sci. U.S.A.*, *102*, 14,683–14,688, doi:10.1073/pnas.0506625102.
Füssel, J., P. Lam, G. Lavik, M. M. Jensen, M. Holtappels, M. Günter, and M. M. M. Kuypers (2012), Nitrite oxidation in the Namibian oxygen minimum zone, *ISME J.*, *6*, 1200–1209, doi:10.1038/ismej.2011.178.
Ganesh, S., L. A. Bristow, M. Larsen, N. Sarode, B. Thamdrup, and F. J. Stewart (2015), Size-fraction partitioning of community gene transcription and nitrogen metabolism in a marine oxygen minimum zone, *ISME J.*, *9*, 2682–2696, doi:10.1038/ismej.2015.44.
Gaye, B., B. Nagel, K. Dahnke, T. Rixen, and K. C. Emeis (2013), Evidence of parallel denitrification and nitrite oxidation in the ODZ of the Arabian Sea from paired stable isotopes of nitrate and nitrite, *Global Biogeochem. Cycles*, *27*, 1059–1071, doi:10.1002/2011GB004115.
Granger, J., and D. M. Sigman (2009), Removal of nitrite with sulfamic acid for nitrate N and O isotope analysis with the denitrifier method, *Rapid Commun. Mass Spectrom.*, *23*, 3753–3762, doi:10.1002/rcm.4307.
Granger, J., D. M. Sigman, M. F. Lehmann, and P. D. Tortell (2008), Nitrogen and oxygen isotope fractionation during dissimilatory nitrate reduction by denitrifying bacteria, *Limnol. Oceanogr.*, *53*, 2533–2545, doi:10.4319/lo.2008.53.6.2533.
Granger, J., D. M. Sigman, M. M. Rohde, M. T. Maldonado, and P. D. Tortell (2010), N and O isotope effects during nitrate assimilation by unicellular prokaryotic and eukaryotic plankton cultures, *Geochim. Cosmochim. Acta*, *3*, 1030–1040, doi:10.1016/j.gca.2009.10.044.
Gruber, N., and J. N. Galloway (2008), An Earth-system perspective of the global nitrogen cycle, *Nature*, *451*, 293–296, doi:10.1038/nature06592.
Gruber, N., and J. L. Sarmiento (1997), Global patterns of marine nitrogen fixation and denitrification, *Global Biogeochem. Cycles*, *11*, 235–266, doi:10.1029/97GB00077.
Hattori, A., and E. Wada (1971), Nitrite distribution and its regulating processes in the equatorial Pacific Ocean, *Deep Sea Res.*, *18*, 557–568, doi:10.1016/0011-7471(71)90122-7.
Holmes, R. M., A. Aminot, R. Kerouel, B. A. Hooker, and B. J. Peterson (1999), A simple and precise method for measuring ammonium in marine and freshwater ecosystems, *Can. J. Fish. Aquat. Sci.*, *56*, 1801–1808, doi:10.1139/f99-128.
Jensen, M., P. Lam, N. P. Revsbech, B. Nagel, B. Gaye, M. S. M. Jetten, and M. M. M. Kuypers (2011), Intensive nitrogen loss over the Omani Shelf due to anammox coupled with dissimilatory nitrite reduction to ammonium, *ISME J.*, *5*, 1660–1670, doi:10.1038/ismej.2011.44.
Kalvelage, T., G. Lavik, P. Lam, S. Contreras, L. Arteaga, C. R. Loscher, A. Oschlies, A. Paulmier, L. Stramma, and M. M. M. Kuypers (2013), Nitrogen cycling driven by organic matter export in the South Pacific oxygen minimum zone, *Nat. Geosci.*, *6*, 228–234, doi:10.1038/ngeo1739.
Kiefer, D. A., R. J. Olson, and O. Holmhansen (1976), Another look at nitrite and chlorophyll maxima in central North Pacific, *Deep Sea Res.*, *23*, 1199–1208, doi:10.1016/0011-7471(76)90895-0.
Kritee, K., D. Sigman, J. Granger, B. B. Ward, A. Jayakumar, and C. Deutsch (2012), Reduced isotope fractionation by denitrification under conditions relevant to the ocean, *Geochim. Cosmochim. Acta*, *92*, 243–259, doi:10.1016/j.gca.2012.05.020.
Kuypers, M., A. Sliekers, G. Lavik, M. Schmid, G. Kuenen, D. Sinninghe, S. Jaap, M. Strous, and M. S. M. Jetten (2003), Anaerobic ammonium oxidation by anammox bacteria in the Black Sea, *Nature*, *422*, 608–611, doi:10.1038/nature01472.
Kuypers, M., G. Lavik, D. Woebken, M. Schmid, B. M. Fuchs, R. Amann, B. B. Jørgensen, and M. S. M. Jetten (2005), Massive nitrogen loss from the Benguela upwelling system through anaerobic ammonium oxidation, *Proc. Natl. Acad. Sci. U.S.A.*, *102*, 6478–6483, doi:10.1073/pnas.0502088102.
Lam, P., G. Lavik, M. M. Jensen, J. van de Vossenberg, M. Schmid, D. Woebken, D. Gutierrez, R. Amann, M. S. M. Jetten, and M. M. M. Kuypers (2009), Revising the nitrogen cycle in the Peruvian oxygen minimum zone, *Proc. Natl. Acad. Sci. U.S.A.*, *106*, 4752–4757, doi:10.1073/pnas.0812444106.
Lam, P., M. M. Jensen, A. Kock, K. A. Lettmann, Y. Plancherel, G. Lavik, H. W. Bange, and M. M. M. Kuypers (2011), Origin and fate of the secondary nitrite maximum in the Arabian Sea, *Biogeosciences*, *8*, 1565–1577, doi:10.5194/bg-8-1565-2011.
Levipan, H. A., V. Molina, and C. Fernandez (2014), Nitrospina-like bacteria are in the main drivers of nitrite oxidation in the seasonal upwelling area of the eastern South Pacific (Central Chile similar to 36 degrees S), *Environ. Microbiol. Rep.*, *6*, 565–573, doi:10.1111/1758-2229.12158.
Lipschultz, F., S. C. Wofsy, B. B. Ward, L. A. Codispoti, G. Friedrich, and J. W. Elkins (1990), Bacterial transformations of inorganic nitrogen in the oxygen-deficient waters of the eastern tropical South Pacific Ocean, *Deep Sea Res., Part A*, *37*, 1513, doi:10.1016/0198-0149(90)90060-9.
Lomas, M., and F. Lipschultz (2006), Forming the primary nitrite maximum. Nitrifiers or phytoplankton?, *Limnol. Oceanogr.*, *51*, 2453–2467, doi:10.4319/lo.2006.51.5.2453.
Lücker, S., B. Nowka, T. Rattei, E. Spieck, and H. Daims (2013), The genome of the Nitrospina gracilis illuminiates the metabolism and evolution of the major marine nitrite oxidizer, *Front. Microbiol.*, *4*, 1–19, doi:10.3389/fmicb.2013.00027.
McIlvin, M. R., and M. A. Altabet (2005), Chemical conversion of nitrate and nitrite to nitrous oxide for nitrogen and oxygen isotopic analysis in freshwater and seawater, *Anal. Chem.*, *77*, 5589–5595, doi:10.1021/ac050528s.
McIlvin, M. R., and K. L. Casciotti (2011), Technical updates to the bacterial method for nitrate isotopic analyses, *Anal. Chem.*, *83*, 1850–1856, doi:10.1021/ac1028984.
Mincer, T. J., M. J. Church, L. T. Taylor, C. Preston, D. M. Kar, and E. F. DeLong (2007), Quantitative distribution of presumptive archaeal and bacterial nitrifiers in Monterey Bay and the North Pacific Subtropical Gyre, *Environ. Microbiol.*, *9*, 1162–1175, doi:10.1111/j.1462-2920.2007.01239.x.
Morrison, J. M., L. A. Codispoti, S. Gaurin, B. Jones, V. Magnhnani, and Z. Zheng (1998), Seasonal variation of hydrographic and nutrient fields during the US JGOFS Arabian Sea process study, *Deep Sea Res., Part II*, *45*, 2053–2102, doi:10.1016/S0967-0645(98)00063-0.
Naqvi, S. W. A., T. Yoshinari, A. Jayakumar, M. A. Altabet, P. V. Narvekar, A. H. Devol, J. A. Brandes, and L. A. Codispoti (1998), Budgetary and biogeochemical implications of N_2O isotope signatures in the Arabian Sea, *Nature*, *394*, 462–464, doi:10.1038/28828.
Olson, R. J. (1981), Differential photoinhibition of marine nitrifying bacteria: A possible mechanism for the formation of primary nitrite maximum, *J. Mar. Res.*, *39*, 227–238.
Rafter, P., P. Difiore, and D. Sigman (2013), Coupled nitrate nitrogen and oxygen isotopes and organic matter remineralization in the Southern and Pacific Oceans, *J. Geophys. Res. Oceans*, *118*, 4781–4794, doi:10.1002/jgrc.20316.
Rotthauwe, J. H., K. P. Witzel, and W. Liesack (1997), The ammonia monooxygenase structural gene amoA as a functional marker: Molecular fine-scale analysis of natural ammonia-oxidizing populations, *Appl. Environ. Microbiol.*, *63*, 4704–4712.
Saito, M. A., G. Rocap, and J. W. Moffett (2005), Production of cobalt binding ligands in a Synechococcus feature at the Costa Rica upwelling dome, *Limnol. Oceanogr.*, *50*, 279–290.
Santoro, A. E., K. L. Casciotti, and C. A. Francis (2010), Activity, abundance and diversity of nitrifying archaea and bacteria in the central California Current, *Environ. Microbiol.*, *12*, 1989–2006, doi:10.1111/j.1462-2920.2010.02205.x.

Santoro, A. E., C. M. Sakamoto, J. M. Smith, J. N. Plant, A. L. Gehman, A. Z. Worden, K. S. Johnson, C. A. Francis, and K. L. Casciotti (2013), Measurements of nitrite production in and around the primary nitrite maximum in the central California Current, *Biogeosciences*, *11*, 7395–7410, doi:10.5194/bg-10-7395-2013.

Sigman, D. M., K. L. Casciotti, M. Andreani, C. Barford, M. Galanter, and J. K. Bohlke (2001), A bacterial method for the nitrogen isotopic analysis of nitrate in seawater and freshwater, *Anal. Chem.*, *73*, 4145–4153, doi:10.1021/ac010088e.

Sigman, D. M., J. Granger, P. J. DiFiore, M. M. Lehmann, R. Ho, G. Cane, and A. van Geen (2005), Coupled nitrogen and oxygen isotope measurements of nitrate along the eastern North Pacific margin, *Global Biogeochem. Cycles*, *19*, GB4022, doi:10.1029/2005GB002458.

Sigman, D. M., P. J. DiFiore, M. Hain, C. Deutsch, Y. Wang, D. Karl, A. Knapp, M. Lehmann, and S. Pantoja (2009), The dual isotopes of deep nitrate as a constraint on the cycle and budget of oceanic fixed nitrogen, *Deep Sea Res., Part I*, *56*, 1419–1439, doi:10.1016/j.dsr.2009.04.007.

Strickland, J. D. H., and T. R. Parsons (1972), *A Practical Handbook of Seawater Analysis*, vol. 167, 310 pp, Ottawa Fisheries Research Board of Canada.

Strous, M., et al. (2006), Deciphering the evolution and metabolism of an anammox bacterium from a community genome, *Nature*, *7085*, 790–794, doi:10.1038/nature04647.

Stukel, M. R., M. Décima, K. E. Selph, D. A. A. Taniguchi, and M. R. Landry (2013), The role of Synechococcus in vertical flux in the Costa Rica upwelling Dome, *Prog. Oceanogr.*, *112–113*, 49–59, doi:10.1016/j.pocean.2013.04.003.

Thamdrup, B., and T. Dalsgaard (2002), Production of N_2 through anaerobic ammonium oxidation coupled to nitrate reduction in marine sediments, *Appl. Environ. Microbiol.*, *68*, 1312–1318.

Thamdrup, B., T. Dalsgaard, and N. Revsbech (2012), Widespread functional anoxia in the oxygen minimum zone of the eastern South Pacific, *Deep Sea Res., Part I*, *65*, 36–45, doi:10.1016/j.dsr.2012.03.001.

Thomas, W. H. (1966), Surface nitrogenous nutrients and phytoplankton in northeastern tropical Pacific Ocean, *Limnol. Oceanogr.*, *11*, 393.

Vaccaro, R., and J. Ryther (1960), Marine phytoplankton and the distribution of nitrite in the sea, *J. Cons. Int. Explor. Mer.*, *25*, 260–271.

Wankel, S., C. Kendall, J. Penninton, F. P. Chavez, and A. Paytan (2007), Nitrification in the euphotic zone as evidenced by nitrate dual isotopic composition: Observations from Monterey Bay, California, *Global Biogeochem. Cycles*, *21*, GB2009, doi:10.1029/2006GB002723.

Ward, B. B. (2013), How nitrogen is lost, *Science*, *341*, 352–353, doi:10.1126/science.1240314.

Ward, B. B., R. Olson, and M. Perry (1982), Microbial nitrification rates in the primary nitrite maximum off southern California, *Deep Sea Res., Part A*, *29*, 247–255, doi:10.1016/0198-0149(82)90112-1.

Ward, B. B., A. H. Devol, J. J. Rich, B. X. Chang, S. E. Bulow, H. Naik, A. Pratihary, and A. Jayakumar (2009), Denitrification as the dominant nitrogen loss process in the Arabian Sea, *Nature*, *461*, 78–81, doi:10.1038/nature08276.

Wyrtki, K. (1962), The oxygen minima in relation to ocean circulation, *Deep Sea Res.*, *9*, 11–23, doi:10.1016/0011-7471(62)90243-7.

Wyrtki, K. (1964), Upwelling in the Costa Rica Dome, *Fish Wildl. Serv.*, *63*, 355–372.

Zafiriou, O. C., L. A. Ball, and Q. Hanley (1992), Trace nitrite in oxic waters, *Deep Sea Res., Part A*, *7-8A*, 1329–1347, doi:10.1016/0198-0149(92)90072-2.